1092–1110 *Nucleic Acids Research, 2022, Vol. 50, No. 2* *Published online 8 January 2022*
https://doi.org/10.1093/nar/gkab1261

Determinants of the temperature adaptation of mRNA degradation

Vincent Jaquet†, Sandrine Wallerich†, Sylvia Voegeli†, Demeter Túrós, Eduardo C. Viloria and Attila Becskei*

Biozentrum, University of Basel, Klingelbergstrasse 50/70, 4056 Basel, Switzerland

Received October 30, 2021; Revised December 04, 2021; Editorial Decision December 06, 2021; Accepted December 09, 2021

ABSTRACT

The rate of chemical reactions increases proportionally with temperature, but the interplay of biochemical reactions permits deviations from this relation and adaptation. The degradation of individual mRNAs in yeast increased to varying degrees with temperature. We examined how these variations are influenced by the translation and codon composition of mRNAs. We developed a method that revealed the existence of a neutral half-life above which mRNAs are stabilized by translation but below which they are destabilized. The proportion of these two mRNA subpopulations remained relatively constant under different conditions, even with slow cell growth due to nutrient limitation, but heat shock reduced the proportion of translationally stabilized mRNAs. At the same time, the degradation of these mRNAs was partially temperature-compensated through Upf1, the mediator of nonsense-mediated decay. Compensation was also promoted by some asparagine and serine codons, whereas tyrosine codons promote temperature sensitization. These codons play an important role in the degradation of mRNAs encoding key cell membrane and cell wall proteins, which promote cell integrity.

INTRODUCTION

Heat increases the velocity of molecular motion, leading to more intense and frequent molecular collisions and consequently, faster reactions. Typically, the rate of enzymatically catalyzed biochemical reactions plateaus or even decreases at higher temperatures because the enzymes denature or their biophysical properties change (1). Biochemical processes can also cause deviations from the simple, linear relation between the temperature and reaction rate. Sensitization brings about larger than expected changes in reaction rates, whereas temperature compensation buffers the temperature-induced changes in a reaction. These two forms of temperature adaptation have been observed in various organisms. Sensitization can be achieved for example with molecular thermometers, which allow the translation of bacterial heat shock and virulence factors to increase abruptly at a threshold temperature (2). Conversely, the response rate of a network with antagonistic reactions can remain constant (3). This temperature compensation is important to maintain constant biological rhythms, neurobiological behavior or animal development over a wide temperature range (3–6).

Little is known whether and how the mRNA degradation, a core process of molecular biology, is subject to temperature compensation, or sensitization. mRNA degradation is strongly affected by translation, and it is therefore plausible that the two processes together determine the temperature-dependence of mRNA stability. The codon composition of mRNAs affects not only translation efficiency but also the mRNA degradation rate (7–9). Typically, codons recognized by abundant tRNAs stabilize mRNAs, whereas codons recognized by scarce tRNAs destabilize mRNAs. Under standard environmental conditions, there is a positive correlation between the frequency of optimal codons in an mRNA and mRNA stability.

The degradation of mRNAs can also be controlled through sequestration or by other means. High temperature or heat-shock promotes the appearance of ribonucleoprotein aggregates, such as P-bodies and stress granules, which have been proposed to act as storage sites of translationally repressed mRNAs (10–12). The stabilization and storage of mRNA in such aggregates could compensate the degradation kinetics due to increases in temperature.

Despite the fact that codon optimality was recognized early on as a major determinant of mRNA stability (13), the confirmation of these initial studies was hindered for a long time by the variable, often inconsistent results of different methods and protocols for measuring half-lives (14–16).

The measurement of half-life under stressful conditions, such as heat-shock, is even more demanding, since the perturbations introduced by different methods imitate and amplify stress response (17,18). In the first part of our work,

*To whom correspondence should be addressed. Tel: +41 61 207 2222; Email: attila.becskei@unibas.ch
†The authors wish it to be known that, in their opinion, the first three authors should be regarded as Joint First Authors.

we were able to measure mRNA half-lives over a wide temperature range with minimal methodological interference. To study how translation affects the temperature response of mRNA degradation, we created mRNAs devoid of start codons to eliminate translation with minimal disruption of cell physiology. We found that heat shock is a special environmental condition in that it reduces the proportion of translationally stabilized mRNAs, a process that is mediated in part by Upf1. Simultaneously, the degradation of these mRNAs becomes temperature compensated, partly by Upf1. We then turned our attention to the intrinsic mRNA determinants and uncovered how codon composition affects temperature compensation and sensitization in mRNA degradation.

MATERIALS AND METHODS

Construction of plasmids and yeast strains

The plasmids constructed in this study are listed in Supplementary Table S1. Plasmids containing an RNA expression cassette include a promoter and a sequence that is identical to or creates the open reading frame (ORF) upon integration into the yeast chromosome. The promoter is a truncated *GAL1* promoter, where the four Gal4p-binding sites were replaced by *tet* operators. The 5′UTR of the gene of interest was inserted 12 bp downstream of the TATA box of the *GAL1* promoter.

Two strategies were used to express the gene of interest in yeast: (1) promoter replacement, resulting in the expression of the gene at the endogenous chromosomal locus and (2) expression of the whole gene at an exogenous locus. In the first strategy, employing promoter replacement, a truncated ORF constituted the homologous sequence for integration to the endogenous locus, and the *URA3* was used as a selection marker (19). The plasmid was linearized typically with SpeI or with other restriction enzymes whose recognition sites were introduced by fusion PCR (as indicated in Supplementary Table S1). In the second strategy, the whole gene along with the 5′ and 3′ UTR flanking the ORF was cloned downstream of the promoter in the pRS303 plasmid, to be integrated at the *his3* locus of yeast. The *his3* locus has a partial deletion in the BY4741/2 strains. The sequence downstream of the ORF contained the 3′UTR and a further 100 bp sequence in order to allow for transcriptional termination as it occurs at the endogenous locus. This second strategy was mainly used for genes that have a short ORF (600 bp or less), contain an intron, are essential or mutations were introduced into the whole coding sequence (see below), as well as for the synthetic genes. The linearization was performed primarily with MscI, but when this restriction site was also present in the gene sequence, BssHII was used. In order to permit the simultaneous measurement of multiple RNA, multiplexing was used with the help of synonymous codon substitution (19).

A second form of multiplexing was used for the genes encoding extreme $\sum$dtCSC values: multiple stop codons were inserted downstream of the endogenous stop codons instead of inserting the synonymous codons. These genes with 3′UTR modifications can be distinguished with qRT-PCR from the endogenous counterparts with repetitive sequences, which is common in serine-rich genes.

To construct the noATG versions of the endogenous genes, all ATGs were replaced by a TAG triplet in all three frames and also in the 3′UTRs in order to prevent translation. The noATG version of the *TSL1* used for the single-molecule RNA FISH was additionally modified to avoid cross-hybridization, which was achieved by swapping the position of the i and $i + 1$ codons and this construct was named as scrambled noATG *TSL1*. These noATG constructs were synthesized by General Biosystems (pGB series) or Biomatik (pBM series) and cloned into pRS303 and integrated according to the second strategy, which is pursued when the insert in the plasmid contains the entire ORF. The codons of the synthetic versions of *MTL1* were replaced as shown in Figure 6A.

The plasmids were chromosomally integrated into *Saccharomyces cerevisiae* BY4741 and BY4742 strains. Single copy integrands were screened with colony PCR and the haploid strains were mated resulting in diploid strains (Supplementary Table S2). Integrated repetitive sequences were also verified by sequencing. The *tet* operators were recognized by the constitutively expressed tTA, driven by the *CLN3* promoter. The haploid strain containing the tTA (Ysv71.1) was mated with the strain containing the RNA expression cassettes. Strains with gene deletions, including the Δ*xrn1* (Y34540) and cell wall mutant strains were obtained from EUROSCARF. The genes are deleted with the kanMX cassette.

The following classes of strains expressing the RNA under TET control were obtained (Supplementary Table S2): (1) RNAs with synthetic codon composition, (2) a set of representative mRNAs, the (3) set of stable and unstable mRNAs and (4) mRNAs with extreme $\sum$dtCSC values.

To obtain a representative set of mRNAs, genes in the segments of the YML and YBR chromosomes were selected. Such a selection provides a faithful estimation of the average half-life and correlations of the genome-wide measurements (19). To increase the power of the predictions, we combined all the YML and YBR genes mentioned in the previous study using multiplexed gene control (19) and the YML and YBR genes listed in Supplementary Table S1. To obtain stable and unstable mRNAs, we selected mRNAs that had very short or long half-lives according to multiple measurements using different methodologies (16,20). The no-ATG counterparts were constructed for this set to estimate the neutral half-life.

Yeast growth and shut-off experiments

Cells were grown in synthetic drop-out medium (Yeast nitrogen base, Formedium). We used either of the three following carbon sources: 2% raffinose (supplemented with 0.005% glucose, reference condition), 2% glucose and 3% Glycerol supplemented with 0.005% glucose. Raffinose is the trisaccharide galactose α(1→6) glucose β(1→2) fructose. The reference temperature was 30°C. We measured decay rates also at 20 and 42°C. The overnight cultures were refreshed at OD600 = 0.1 and let further grown until they reached an OD600 ∼ 0.5 unless otherwise specified. For growth in glycerol, the OD600 after refreshment was adjusted to 0.5, and the culture was grown for 4 h before starting the decay experiment. For the measurement at 42°C,

cultures were grown overnight and initially after refreshment at 30°C. After reaching the mid-log phase (optical density at 600 nm, $OD_{600} \sim 0.5$), the cells were filtered through a cellulose acetate membrane and then transferred into a new medium at 42°C. The culture was grown for 30 min before starting the decay measurement by adding the doxycycline.

Up to 20 cultures were pooled to measure the decay rate of multiple mRNAs simultaneously (19). Gene expression was shut off by adding doxycycline at a final concentration of 10 μg/ml to dissociate tTA from the promoter. Samples were collected before and 2, 4, 6, 8, 12, 18, 24, 36, 48 and 64 min after the addition of doxycycline unless otherwise specified. The samples were fixed by pouring them into the same volume of methanol cooled in dry ice.

RT-qPCR

Total RNA isolated from the cells was used to quantify mRNA. RT-qPCR was performed with gene specific primers (Supplementary Table S3). The 15aa repetitive sequences containing 15 identical codons had a low efficiency amplification. For these constructs, we used RT-qPCR with barcoding, in a way that a barcode sequence incorporated into the reverse transcription primer was recognized by reverse primer in the qPCR instead of annealing directly to the repeat sequence.

Calculation of mRNA half-lives

The half-lives were fitted as described earlier (19). The mean decay rate constant (or half-life) was calculated from at least two independently fitted decay rates obtained from biological replicates. Three replicates were performed always for the mRNAs with synthetic codon composition and extreme $\sum$dtCSC values. Otherwise, we performed more than two replicates if the determination of the half-lives did not meet the criteria based on the dynamic range or experimental variability. The dynamic range of expression was defined as the ratio of maximal to the minimal value in the time series. If the dynamic range was <5, the time series was replaced by a new replicate experiment. If the dynamic range remained below 5, the half-life was not measured for that construct. The experimental variability was quantified with the coefficient of variation (CV). If the CV of two replicates was above 0.5, additional replicates were performed. Outliers that were greater than twice the mean absolute difference (2 MAD) were removed from the representative mRNA data set (21) to achieve high precision in the input data. The 2 MAD criterion was not applied to data with error bars for which conclusions were drawn.

Splinted ligation RT-qPCR (qSL-RT-PCR)

Total RNA isolated from exponentially growing cells was used for the splinted ligation, which was performed as described earlier (22) with a few modifications. Since the splint can promote the ligation of only one mRNA isoform with a given 5′UTR length, we selected the most frequent 5′UTR length, having 31, 16 and 34 bp, for the *YBR025C*, *YJL190C* and *YLR094C* 5′UTRs, respectively (23). The primers were designed to avoid cross-reaction with the endogenous mRNA (Supplementary Figure S4 and Supplementary Table S4). The increased specificity was achieved by having anchor forward primers that overlapped with the 5′UTR of the gene over a few base pairs and by using distinct primers annealing to different sequences in the reverse transcription and in the qPCR. The primers for RPL41A were the same as previously described (22) except for the anchor forward PCR primer, which was designed as described above. The RNA ligation reaction was performed with T4 DNA ligase (Promega), and the RNA was purified with RNeasy MinElute Cleanup Kit (Qiagen) upon the completion of the ligation reaction. Reverse transcription and qPCR were performed as described in the RNA quantification section.

Decapping was performed with the 5′ Pyrophosphohydrolase enzyme RppH (NEB) in the NEB2 buffer for 90 min at 37°C. The reaction was stopped by adding EDTA and heating it to 65°C for 5 min. The RNA was purified from the reaction mixture with RNeasy MinElute Cleanup Kit (Qiagen).

The percentage of the decapped RNA is calculated by dividing the amount of the mRNA ligated to the anchor RNA (mRNA – anchor RNA hybrid) by the total RNA amount. This raw value was normalized by the bulk ligation efficiency to obtain the final value of the decapped RNA percentage. The ligation efficiency is assessed by performing the SL-RT-qPCR on the mRNA decapped with RppH, and it is affected by the efficiency of ligation of a given mRNA isoform as well as by the proportion of the isoform in the RNA population to be measured with respect to the total RNA, which comprises all RNA isoforms.

$$\begin{aligned}&\mathrm{DecappedRNA[\%]}\\&= \frac{\mathrm{mRNA-anchorhybrid}}{\mathrm{TotalRNA}} \Big/ \frac{\mathrm{InvitrodecappedmRNA-anchorRNAhybrid}}{\mathrm{InvitrodecappedTotalRNA}} =\\&= \frac{\mathrm{SL-RT-qPCR(RNA)}}{\mathrm{RT-qPCR(RNA)}} \Big/ \frac{\mathrm{SL-RT-qPCR(decappedRNA)}}{\mathrm{RT-qPCR(decappedRNA)}}\end{aligned}$$

The (SL)-RT-qPCR values were calculated from the *C*p values and the amplification efficiency. The primers were designed to maximize the signal-to-noise ratio. This ratio was calculated by dividing the amount of the mRNA-anchor hybrid RNA molecule detected in a reaction containing a ligase by that detected in the mock reaction without ligase:

$$\mathrm{Signal-to-noiseRatio} = \frac{\mathrm{InvitrodecappedmRNA-anchorRNAhybrid}}{\mathrm{InvitrodecappedmRNA-anchorRNAhybrid(withoutT4ligase)}}$$

Single-molecule RNA FISH

The microscopic slides of the sample were prepared according to Stellaris® RNA protocol for yeast (24,25), with a few modifications. Following the fixation with formaldehyde, the cell wall was digested with zymolyase at 37°C for 15 min in spheroblast buffer. Following the hybridization, the cells were placed on slide using the ProLong™ Glass Antifade Mountant (ThermoFisher) mounting medium. The images were acquired as previously described (19). Two sets of probes were designed to bind either the WT or the scrambled noAUG sequence variants of the 5′ region of the *TSL1* RNA. Both sets comprehended 35 probes labeled at their 3′ end with Quasar® 670 (Stellaris probes). The

probe length was adjusted between 18 and 22 bp to have a melting temperature of 55°C and a gap of at least 2 bp in the complementary sequences between each probe (Supplementary Table S5). Microscopy data are stored as multichannel (Quasar 670 RNA probe, DAPI, autofluorescence at 523 nm) image stacks. Each stack consists of 20–25 slices and approximately 15 field of views have been imaged for each experimental condition.

Mass spectrometric analysis of protein abundance

Cells were harvested 3 h after shifting the culture to 42°C. Cells were processed as described earlier (26). Synthetic peptides (Data S2) were used for the quantification of relative changes in protein abundance by selective reaction monitoring.

Image analysis

To segment cell bodies, the Cellpose Python Package (Python 3.8.5) was utilized in a cloud-based Python environment with GPU support provided by Google Colaboratory (27). Each image plane in a stack was segmented using the Cellpose 2D segmentation algorithm with the diameter parameter set to 70. After completion, the corresponding 2D segmentation masks were merged together forming a 3D binary mask for each individual cell in each image stack. Too small or too big cell bodies have been removed as well as cells touching the image boundaries. The DAPI-labeled cell nuclei were segmented by separating the pixels into two classes using Otsu's method and creating a binary image by multiplying the threshold value by 1.9 with subsequent manual validation. Too small regions have been discarded. Next, we computed the Euclidean distance between the centroid of each cell and each nucleus and paired them according to the smallest distance value. Cells with no visible nuclei were omitted from further analysis.

In order to quantify the RNA spots, the binary cell body masks were applied and the mean cell volume intensity was calculated for each field of view on the previously deconvolved Quasar 670 image channels. Individual RNA spots were selected by employing a threshold value corresponding to the mean cell intensity multiplied by 5.0. This approach was consistent across strains since the mean cell intensity did not change >1.3 times upon subtracting the RNA spots. Next, the numbers of RNA spots in the cytoplasm and nucleus were counted for each cell.

Quantification of cell wall integrity

The cell wall integrity was assessed by exposing the cells to a mixture of glucanases (zymolyase) that degrade the cell wall, yielding spheroblasts, cells devoid of cell wall. The susceptibility of cells to lysis was quantified according to the spheroblast rate assay (28), with a few modifications.

To obtain cells in exponential growth phase, overnight cell cultures were grown at 30°C in minimal medium containing 2% raffinose. The overnight culture was diluted to an OD600 of 0.15 (0.25 for slow-growing strains), and incubated for 5 h at 30°C. In this way, the culture did not exceed an OD600 of 0.5, allowing the analysis of cells in a mid-exponential growth phase. The culture at 42°C was also incubated for 5 h, which was preceded by a growth for 2 h at 30°C following the dilution of the overnight culture grown at 30°C.

The cells in the mid-exponential growth-phase were pelleted and washed three times with 30°C Tris-EDTA (TE) buffer. The cells were then resupended in 1 ml of TE buffer to an OD600 of 0.6. The enzymatic reaction was started by adding 25 μg/ml zymolyase (Zymolyase 20T (Arthrobacter luteus) amsbio #120491–1) to 1 ml of cell suspension. The progress of spheroblast lysis was monitored by recording OD600 at intervals ranging from 3 to 8 min.

The exponential phase of the lysis begins after a lag. The zymolyase rate index (zymolyase RI, ZRI) was calculated from the lag time (LT) and the maximal lysis rate (MLR).

$$ZRI = \frac{MLR}{LT}$$

The MLR was fitted in the interval starting from the latest time point at which the OD600 remained above a threshold defined as (maximum (OD600)) – 0.05. The MLR corresponds to the maximal slope of any 8 or 10 consecutive time points in the time period after the lag for the 30 and 42°C conditions, respectively. If there are less points than this number of points in the decay phase, all these points are fitted. If the decay rate was too slow to be determined, then it was replaced with the lowest measured experimental rate. The MLR is calculated using linear regression from the logarithmically transformed values. The LT corresponds to the intersection point of the lines defined by the MLR and the maximum (OD600) – 0.05 (Supplementary Figure S8).

Calculation of the differential temperature codon stabilization coefficient (dtCSC)

The relative difference of the RNA half-lives measured at 20 and 42°C (Supplementary Data S1) was used to calculate the dtCSC for each codon.

$$d_r t_{1/2} = \frac{t_{1/2}20°C - t_{1/2}42°C}{\frac{t_{1/2}20°C + t_{1/2}42°C}{2}}$$

The dtCSC is equal to the Pearson rho correlation between the frequency of a specific codon in the mRNAs and the relative difference of the respective half-lives, $d_r t_{1/2}$, unless otherwise indicated. The frequency of the codon was calculated with the Biostrings package in R from Saccharomyces Genome Database (SGD) sequences (29). The number of mRNAs included in the calculation ($N = 95$) encompassed the set of representative mRNAs and the set of stable and unstable mRNAs.

The number of synonymous mutations among all codons is <1% in the multiplexed gene dataset, and consequently, it has minimal impact on the dtCSC values (Supplementary Figure S6A,B): the dtCSC calculated with and without the synonymous mutations, which differentiate the controlled genes from the endogenous genes, are highly correlated (0.99).

The $\sum$dtCSC is the scalar product of the codon frequency and the corresponding dtCSC. The dtCSC was calculated from a smaller set of genes ($N = 81$) to select genes

with extreme ∑dtCSC values. Genes were ranked according to the ∑dtCSC values to select the genes with extreme ∑dtCSC values. The following genes were eliminated from this list: genes that have uncharacterized ORF, unknown function and mitochondrial genes encoded by the mitochondrial genome. Genes enriched in both Tyr and Asn/Ser codons (above the 95 percentile in the codon frequency distribution) were also eliminated because of the dominance of codons that do not have significant dtCSCs. The remaining genes with extreme ∑dtCSC values were cloned (Supplementary Figure S6C, D).

RESULTS

Temperature dependence of mRNA turnover

To examine the temperature dependence of mRNA turnover, we measured the half-life of a representative set of mRNAs in the eukaryotic model organism budding yeast. Cells were grown in media containing the trisaccharide raffinose at low (20˚C), intermediate (30˚C) and high (42˚C) temperatures. For the high temperature growth, the cells were subjected to heat shock: we first cultured the cells at 30˚C and measured the mRNA half-life 30 min after raising the temperature to 42˚C. We used the gene control method to determine the half-lives (see Materials and Methods) since the applied doxycycline introduces minimal stress (30). Thus, it is well suited to study mRNA turnover in different environmental conditions, including heat-stress. The median mRNA half-life shortens as the temperature increases ($t_{1/2}$ = 3.4 min at 20˚C, 2.0 min at 30˚C and 1.5 min at 42˚C) (Figure 1A, B).

mRNAs are degraded 5′→3′ by Xrn1 and 3′→5′ by the exosome but the overall degradation rate is also influenced by the preceding molecular steps, such as the removal of polyA tail and decapping (31). In order to examine the temperature dependence of degradation per se, we monitored RNA degradation in vitro by adding the purified yeast exonuclease Xrn1 to total RNA (Text S1). Xrn1 is a major determinant of differential mRNA stability (19,20,31). We fitted the half-life of the 18S RNA, because it is not 5′-capped and thus, Xrn1 can bind to the RNA without pretreatment (32). The half-life of the 18S RNA decreased with increasing temperature between 20 and 42˚C (Supplementary Figure S1).

The relatively large correlation between the half-lives (Figure 1C) indicates that mRNA turnover responds coherently and gradually to temperature. To examine the coupling of mRNA turnover to cellular metabolism, we measured the growth rate. The cells grew faster at 30˚C than at 20˚C but raising the temperature further to 42˚C did not increase the growth rate in spite of the faster RNA turnover (Figure 1B). After the temperature shift from 30 to 42˚C, the growth rate declined considerably with longer cultivation: the cells grew initially exponentially but after one day of culturing, the growth came to a halt (Supplementary Figure S2). These results indicate that central processes of gene expression, including RNA degradation and translation, persist for a sufficiently long period and permit cells to undergo a few, around three cell divisions before they enter a quiescent state.

Cell growth, RNA nucleocytoplasmic export and degradation stop ultimately upon heat shock; the exact temperature and time at which this ensues varies with growth conditions (33–35). Typically, slower growth results in superior thermotolerance. Heat shock is often studied in cells cultured in glucose, resulting in high-flux fermentation and ethanol accumulation, which can cause further stress (36). These factors may explain why growth in raffinose permits a few cell divisions at 42 ˚C before cells enter cellular quiescence.

In contrast to our results, a mild heat shock (37˚C) has been reported to increase mRNA half-lives in two studies using metabolic labeling (cDTA) and genomic run-on (GRO) (20,37). The two datasets (cDTA, GRO) did not correlate with each other (Figure 1D). The 30˚C dataset of the metabolic labeling study (cDTA) did correlate highly with our multiplexed gene control (MGC) dataset (19) implying a high inter-method reliability. On the other hand, the heat-shock cDTA dataset did not correlate with the 30˚C cDTA dataset and with our MGC datasets (Figure 1D), which suggests that our data reflect the physiologically unperturbed and gradual response of the mRNA turnover to temperature changes, allowing cells to grow and divide.

Analysis of translation-dependence of mRNA degradation with no-AUG mRNAs

Next, we analyzed the translation-dependence of mRNA decay in different conditions, including heat-shock. Translation inhibitors perturb cell physiology and mRNA decoding (31). To circumvent the use of inhibitors, we created mutant genes devoid of start codons (Figure 1E). Genes encoding mRNAs with extreme half-lives, i.e. a set of stable and unstable mRNAs was selected for the mutation. At 20˚C, the mRNAs assumed relatively uniform half-lives when translation was diminished or abrogated due to the mutations. We calculated the interdecile ratio to assess the dispersion, which equals the ratio of 90th to 10th percentile of the half-life distribution. Indeed, the no-AUG mRNAs spanned a much narrower range of half-lives (interdecile ratio: 2.3) in comparison to their WT counterpart (interdecile ratio: 11.4) (Figure 1E).

We quantified the degree of translational stabilization by dividing the half-lives of the mRNAs by that of the no-AUG mRNAs. There is a very strong correlation between mRNA half-life and translational stabilization (Pearson correlation coefficient $\rho = 0.88$, Spearman rank correlation $r_S = 0.90$, Figure 1F). This finding confirms that translation is a major determinant of mRNA stability.

Comparison of the molecular and kinetic properties of no-AUG mRNAs to their AUG counterparts

Before analyzing the temperature response of no-AUG mRNAs, we tested whether they preserve the main features of mRNA processing and degradation.

mRNAs are degraded primarily in the cytoplasm (31). Thus, we assessed first their cellular distribution. The single-molecule RNA FISH images indicate that both the WT and no-AUG mRNAs have similar distribution at 30˚C as well as 30 min after shifting the temperature to 42˚C (Figure 2A–C). The majority of molecules are in the cytoplasm and the

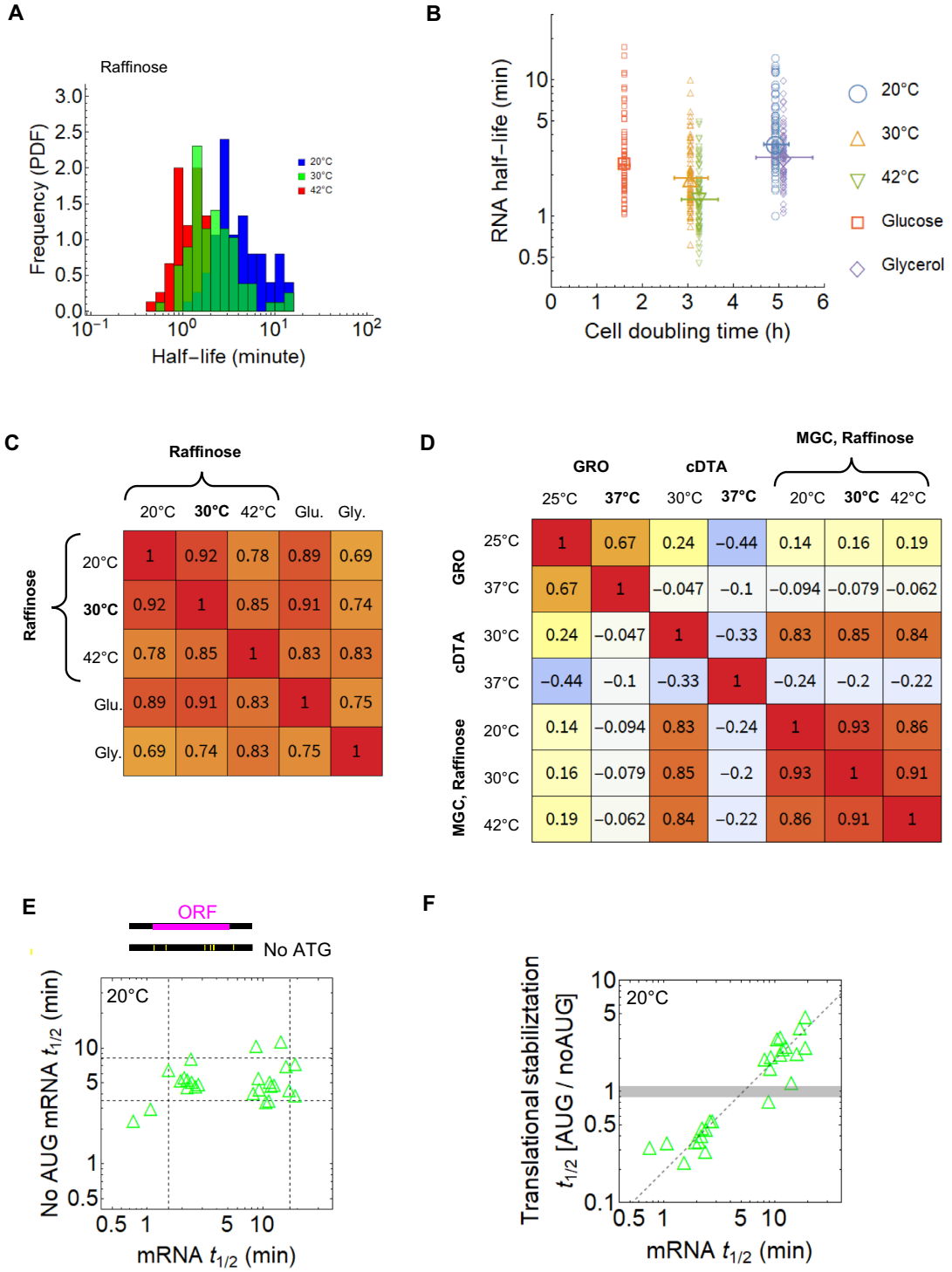

Figure 1. Dependence of mRNA half-lives on temperature, carbon source and translation. (**A** and **B**) The cells were grown in 2% raffinose at 20°C ($N = 75$), 30°C ($N = 78$) or 42°C ($N = 75$), or in 2% glucose ($N = 67$), and 3% glycerol ($n = 69$) at 30°C. The representative set of mRNAs are encoded by genes in the II (YBR) and XIII (YML) chromosomes (Materials and Methods). The distribution of half-lives (A). The half-lives plotted against cell doubling time (mean and standard error from three replicate measurements of the BY4743 strain); the time series of culture density measured over 6 h was used to fit the doubling time by linear regression (B). (**C**) The Spearman's rank correlation (r_S) between the half-lives of the mRNAs in different culturing conditions (data as in A). (**D**) The r_S between the half-lives of mRNAs present in all datasets ($N = 82$). The median half-lives ($N = 82$) are 23.1 min (GRO, 25°C), 27.7 min (GRO, 37°C), 13.3 min (cDTA, 30°C) and 20.6 min (37°C). The GRO 37°C half-lives were calculated from the mRNA amounts and transcription rates measured 40 min after the heat shock. (**E**) The no-ATG genes were constructed by converting all ATG triplets into TAG within the ORF and UTRs (diagram). The half-lives of the set of stable and unstable mRNAs and their no-AUG counterparts in cells grown at 20°C. The dashed lines indicate the position of the lowest and highest deciles (1.5 and 17.1 min for the set of stable and unstable mRNAs and 3.5 and 8.2 min for the no-AUG counterparts). (**F**) The translational stabilization is the ratio of the half-lives of normal (AUG) to that of no-AUG mRNAs. The domains of stabilization (ratio > 1) and destabilization (ratio < 1) are separated by a thick gray line (ratio = 1, no effect of translation). Data identical to those shown in (E).

nascent RNA is visible in the nucleus (Figure 2B,C, Supplementary S3). The number of RNA molecules declines substantially both in the cytoplasm and nucleus after an overnight growth at 42˚C (Figure 2C). This decline is consistent with the cessation of growth of cells exposed to elevated temperature over longer periods of time (Supplementary Figure S2).

Second, we examined the initiation of 5′→3′ degradation. The 5′cap protects the mRNA from the Xrn1 exonuclease, and decapping must precede the 5′→3′ degradation. To assess the 5′ capping state of the mRNAs, we performed splinted-ligation qPCR (qSL-RT-PCR, Methods). qSL-RT-PCR is typically performed with RNA isolated from Δ*xrn1* cells, in which the 5′→3′ exonuclease activity is absent, and the decapped mRNAs accumulate (22,38). With a minor modification of the SL-qPCR protocol, we attained a high-signal-to-noise ratio (Figure 2D) and were able to measure the percentage of the decapped mRNAs even in WT cells in which the decapped mRNAs do not accumulate because Xrn1 rapidly degrades the decapped RNAs (Figure 2E). In Δ*xrn1* cells, around 10% of the *RPL41A* mRNA (*YDL184C*) was decapped, similar to the value reported in the study using the original protocol (22), and we therefore used it as positive control. Rpl41a is a micro-protein in the large subunit of the ribosome, consisting of 25 amino acid residues (39). We also quantified the decapping of the stable (*YBR025C*, *YJL190C*) and unstable (*YLR094C*) mRNAs. In Δ*xrn1* cells, the percentage of decapped mRNAs ranged from 5 to 15%. The values were considerably lower in WT cells. Importantly, the decapping percentages of normal, endogenous and MGC mRNAs (0.2–0.6%) and their RNA counterparts without AUG (0.3–0.6%) were in a similarly low range.

The neutral point defines the half-life above which mRNAs are stabilized by translation

The above results indicate that the no-AUG mRNAs preserve key molecular characteristics of mRNA turnover, specifically the intracellular distribution and the decapping rates (Figure 2), which makes them suitable for quantifying the half-life of untranslated mRNAs. The translation stabilization quotients suggest that translation stabilizes the stable mRNAs but destabilizes the unstable mRNAs (Figure 1F). This dichotomy is interesting because most studies with translation inhibitors suggest that translation is solely stabilizing (31). To characterize this dichotomy in more detail, we calculated the average half-life of the no-AUG mRNAs, which we termed the neutral point. The neutral point of the no-AUG mRNAs marks the neutral half-life of the normal (AUG containing) mRNAs. Translation stabilizes mRNAs above the neutral half-life but destabilizes them below this (Figure 3A).

We calculated the neutral point for different conditions. In cells grown in raffinose at 30˚C, the neutral point is 3.3 min. The equivalent neutral half-life divides the representative set of mRNAs into two subpopulations, with around 22% of the mRNAs being stabilized by translation (Figure 3A). Interestingly, the percentage of mRNAs stabilized by translation was similar (20–25%) for all carbon sources at 30˚C despite the considerably slower growth in glycerol in comparison to glucose (Figures 1C and 3B). That is, even nutrient limitation due to growth on a suboptimal carbon source, glycerol, does not alter this proportion. Only the high-temperature condition (42˚C in raffinose) lead to a substantial change; in this case, a very small fraction of the mRNAs was stabilized by translation (5%, Figure 3A, B). This strong destabilizing effect of mRNA translation may contribute to the cessation of growth upon multiple rounds of cell division at 42˚C.

Upf1 promotes the stability of no-AUG mRNAs after heat shock

To confirm that the neutral point is an unbiased estimate of the neutral half-life, we wanted to examine if residual translation affects the decay of no-AUG mRNAs. Translation is normally initiated at AUG codons but some mRNAs can initiate non-canonical translation at degenerate start codons at a very low rate (40,41). In certain sequence contexts, this rate can reach around one-tenth of the canonical initiation (42). Furthermore, non-canonical translation can become more widespread under specific conditions in yeast, for example, during meiosis, which occurs during sporulation (43). Any such translation would terminate at an early stop codon as we mutated AUGs to UAG codons, resulting in a large the number of stop codons in all reading frames. Such premature translational termination is expected to induce nonsense-mediated decay (NMD). Since NMD is mediated by Upf1, the deletion of *UPF1* stabilizes the mRNAs subject to premature translational termination and thereby increases their abundance (43–45). Using *upf1Δ* cells, we tested whether non-canonically initiated translation gains in importance at low and high temperatures and whether it influences RNA degradation.

No significant difference was observed between the half-lives in WT and *upf1Δ* cells at 20˚C (P-value = 0.42, sign test). Only one of the no-AUG mRNAs was stabilized more than two times in *upf1Δ* cells (Figure 4A). This frequency of NMD targets, around 5%, is in good agreement with the previous finding that 5% of ribosome footprints are due to non-canonical translation in vegetative cells (46). In wild-type cell background, the half-lives of the no-AUG mRNAs are strongly correlated at lower temperatures ($r_S = 0.87$ between 20 and 30˚C, P-value = $2.6{\cdot}10^{-8}$), but they change their behavior in response to heat shock as evidenced by the loss of correlation between 30˚C and 42˚C ($r_S = 0.16$, P-value = 0.46). It turned out that this change was *UPF1*-dependent: we observed a significant difference between the mean mRNA half-lives in WT and *upf1Δ* cells at 42˚C (P-value = 0.0015, sign test). Contrary to expectations, most of the no-AUG mRNAs were destabilized—and not stabilized—in the *upf1Δ* cells (Figure 4B). Typically, the RNAs with the longest half-lives underwent the strongest stabilization, as evidenced by the large correlation (ρ = 0.82) between the half-lives measured in WT and the stabilization ratio due to Upf1. Accordingly, the half-lives became more uniform in *upf1Δ* cells (interdecile ratio = 1.8). These findings suggest that the Upf1 promotes the stability of some no-AUG mRNAs, directly or indirectly. The 20-to-42˚C ratio of average mRNA half-life calculated from the set of stable and unstable mRNAs is 2.39. The ratio de-

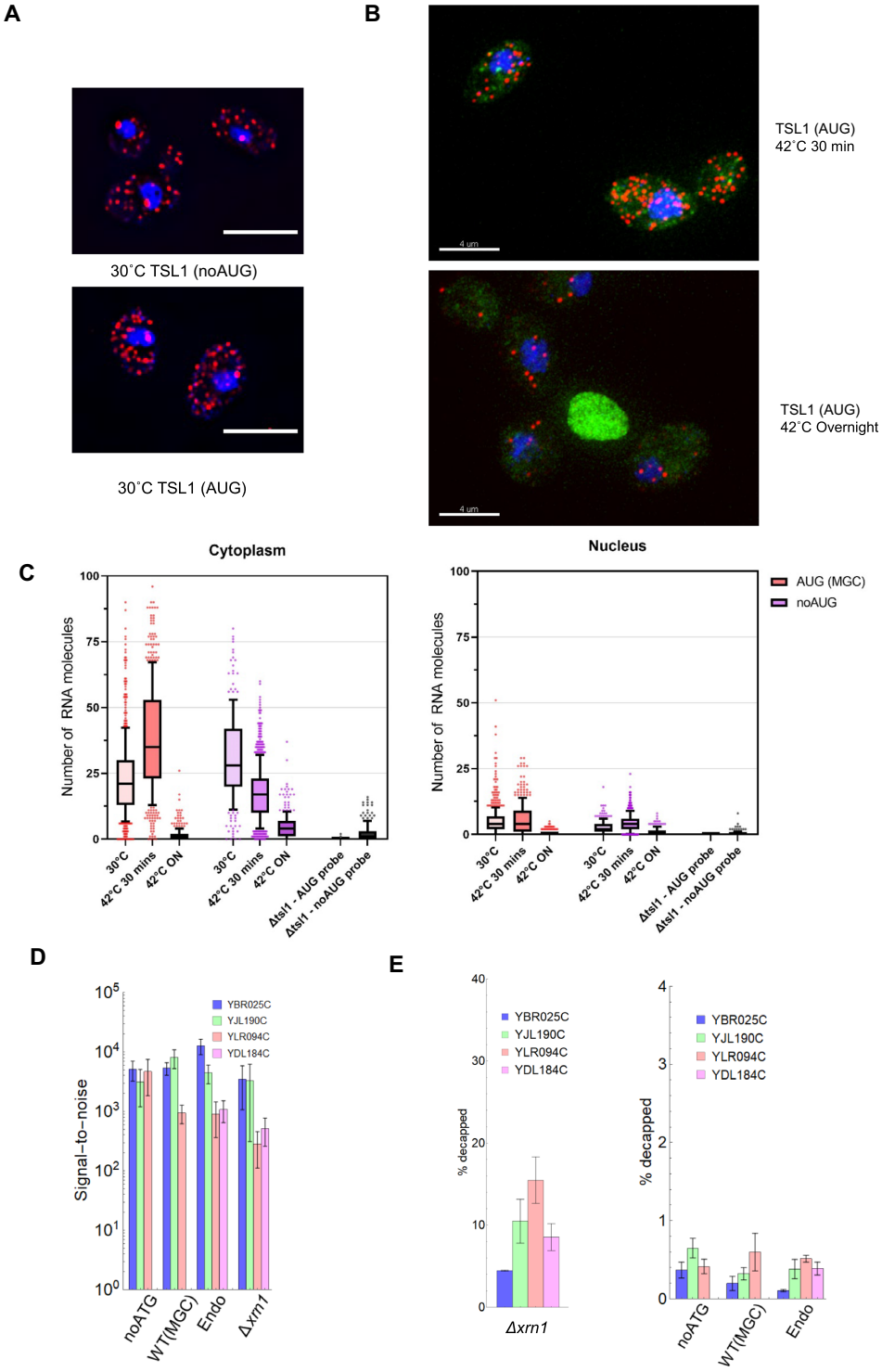

Figure 2. Cellular distribution and the decapping of AUG and no-AUG RNAs. (**A**) smFISH images showing the cellular distribution of the *TSL1* mRNA with and without AUG in cells grown at 30˚C; scale bar, 5 μm. (**B**) Cells grown at 42˚C; in addition to the RNA molecules (red) and DAPI stained nuclear and mitochondrial DNA (blue), the background fluorescence is shown (green). The intense background fluorescence (green) indicates dead cells. (**C**) Number of RNA molecules in the cytoplasm and nucleus at 30˚C, 42 ˚C after 30 min or overnight (ON) incubation. The data for each condition are combined from two or three biological replicates. The boxes and whiskers denote the 25th to 75th and the 10th to 90th percentiles, respectively. The Δ*tsl1* cells hybridized to the *TSL1* (AUG) and no-AUG *TSL1* probes serve as negative controls. The distribution of number of RNA molecules was obtained from *N* cells: *N*(Δtsl1, AUG probe) = 87, *N*(Δtsl1, noAUG probe) = 254, *N*(AUG, 30°C) = 558, *N*(AUG, 42°C 30 min) = 472, *N*(AUG, 42°C ON) = 343, *N*(noAUG, 30°C) = 239, *N*(noAUG, 42°C, 30 min) = 777, *N*(noAUG, 42°C ON) = 270. (**D**) The signal-to-noise ratio of the SL-qPCR assay (see Materials and Methods for the definition). Endo: endogenous genes, Δ*xrn1*: endogenous mRNAs in Δ*xrn1* cells, WT(MGC): 4 silent mutations in ORF, same construct as the one used to determine decay rate. (**E**) Percentage of decapped mRNA measured with the SL-qPCR assay. Error bars: standard error ($n = 3$).

creases to 1.37 when translational initiation is eliminated but returns to near the original number in the *upf1Δ* cells (2.26). These findings suggest that Upf1 is a major determinant of the stabilization of no-AUG mRNAs at 42˚C, a function not classically associated with NMD.

Temperature dependence of mRNA degradation by Upf1

Since the stabilization of no-AUG mRNAs by Upf1 shifts the neutral point, we examined the direct effect of Upf1 on mRNA turnover. We measured the half-life of the set of stable and unstable mRNAs in *upf1Δ* cells (Figures 4C–E). At 30˚C, there was no significant difference between the WT and *upf1Δ* cells (P-value = 0.21, sign-test). Only one of the 23 mRNAs was stabilized more than two times (Figure 4E). In contrast, Upf1 had a specific effect on the decay at 20 and 42˚C. At 20˚C, the mRNAs were slightly but significantly destabilized by *UPF1* (P-value = 0.01, sign test), accelerating the decay across the entire range of half-lives (Figure 4C). At 42˚C, the strong positive correlation between the half-life and the *UPF1* stabilization ratio (USR) indicates a preferential destabilization of unstable mRNAs by *UPF1* (Figure 4D).

To assess whether the temperature rise moderates *UPF1* activity, we calculated the USR(42˚C):USR(20˚C) ratio. This ratio correlates positively with the mRNA half-life at 30˚C (Figure 4F). The ratios calculated for mRNAs at 42˚C above the neutral point (4 min) were significantly higher than one (P-value = 0.012, signed-rank test), indicating that heat shock suspends the destabilizing activity of Upf1 against the mRNAs in the subpopulation stabilized by translation. To examine how Upf1 activity affects temperature adaptation, we calculated the correlation between the USR(42˚C):USR(20˚C) ratio and the relative difference of the half-life measured at 20 and 42˚C ($d_r t_{1/2}$, Materials and Methods). A significant negative correlation ($r_S = -0.49$, P-value = 0.016) indicates that *UPF1* contributes to temperature compensation of mRNA degradation.

Few specific codons are associated with the temperature compensation in mRNA degradation

After identifying the extrinsic determinants, the translation and *UPF1*-dependence of the temperature control of mRNA degradation, we turned to the intrinsic determinants, the codon composition. Codons explain a large proportion of variation in the mRNA half-lives under standard conditions, and mRNAs enriched in certain codons have longer half-lives (8,16). The codon stability coefficient (CSC) indicates how strongly a codon contributes to mRNA stability, and is calculated exactly as the correlation coefficient between the codon frequency and half-life (15,16). Codons with positive CSC stabilize mRNAs whereas those with negative values destabilize them. The CSC is a consistent measure, confirmed by specific variants of all three major methods used to measure RNA stability (15), including the multiplexed gene control (19), the method employed in this study.

The most stabilizing and destabilizing codons that we identified at 20 and at 42˚C (Supplementary Figure S5) correspond to the stabilizing and destabilizing codons previously identified at the standard growth temperature (30˚C) (15,16), which indicates that the degradation code in general withstands temperature variations. In order to identify codons that respond to a temperature shift, we defined a related measure, the differential temperature CSC (dtCSC), which is the correlation coefficient between the codon frequency and the relative difference in the half-lives measured at two different temperatures (Supplementary Figure S6A, B). Unlike CSC, which implies a single condition, the dtCSC always refers to two conditions. The dtCSC values indicate that only few codons contribute significantly to the differential stability at 20 to 42˚C (Figure 5A). Some codons for asparagine and serine dampen the response of mRNA degradation to the temperature shift, and thus promote temperature compensation (negative dtCSC). Conversely, a codon for tyrosine was associated with sensitizing RNA degradation rates to the temperature shift (positive dtCSC).

We tested the above correlations by creating synthetic minigenes containing Asn and Ser codons with the most negative dtCSC. As a control, we used codons with positive dtCSC. Upon the shift of temperature from 20 to 42˚C, the half-life of the control mRNA was halved (Figure 5B). Conversely, the half-life of mRNA composed of codons for Asn and Ser remained essentially unchanged. This reveals that a complete temperature compensation in RNA degradation can be attained with appropriate codons. We also studied coding sequences with homogeneous codon composition containing 15 identical codons. Barcoded primers were used to detect these repetitive sequences in the RT-qPCR (see Materials and Methods). The half-lives of mRNAs consisting of Asn (AAC) and Ser (UCA) codons were in agreement with the previous findings on the temperature compensation, whereas that of the Tyr (UAU) codon was in agreement with the temperature sensitization in mRNA degradation (Figure 5C). The Ser (UCC) and the Leu (CUU) codons had intermediate effect.

Next, we designed longer synthetic genes that encode proteins of 100 amino acids. Long, repetitive sequences of Asn and Ser codons were avoided by adding other codons with negative dtCSC (Supplementary Figure S7). Two similar Ser/Asn rich sequences were designed: SN-rich 1, 2 (Supplementary Figure S7). The SN-rich 1, 2 mRNAs attenuated the temperature response better than a long control mRNA lacking codons for Asn and Ser. The same open reading frame yielded different absolute values for the half-lives in the context of two different flanking UTR sequences (*NRG2* and *RPS22A*). At the same time, the temperature compensation was observed in both contexts (Figure 5D). The SN-rich 1 mRNA displays a 1.73-fold temperature compensation relative to the control mRNA.

The role of temperature degradation code in the turnover of mRNAs encoding key cell membrane and cell wall proteins

Since there are only few codons with compensating or sensitizing effect, the enrichment of mRNAs in these codons is expected to promote temperature adaptation in specific cellular processes. Ser-rich proteins are overrepresented in cell wall and other cell membrane related components (47). Stress granules and P bodies are enriched in Asn-rich or Gln-rich proteins or protein domains, and a weaker positive

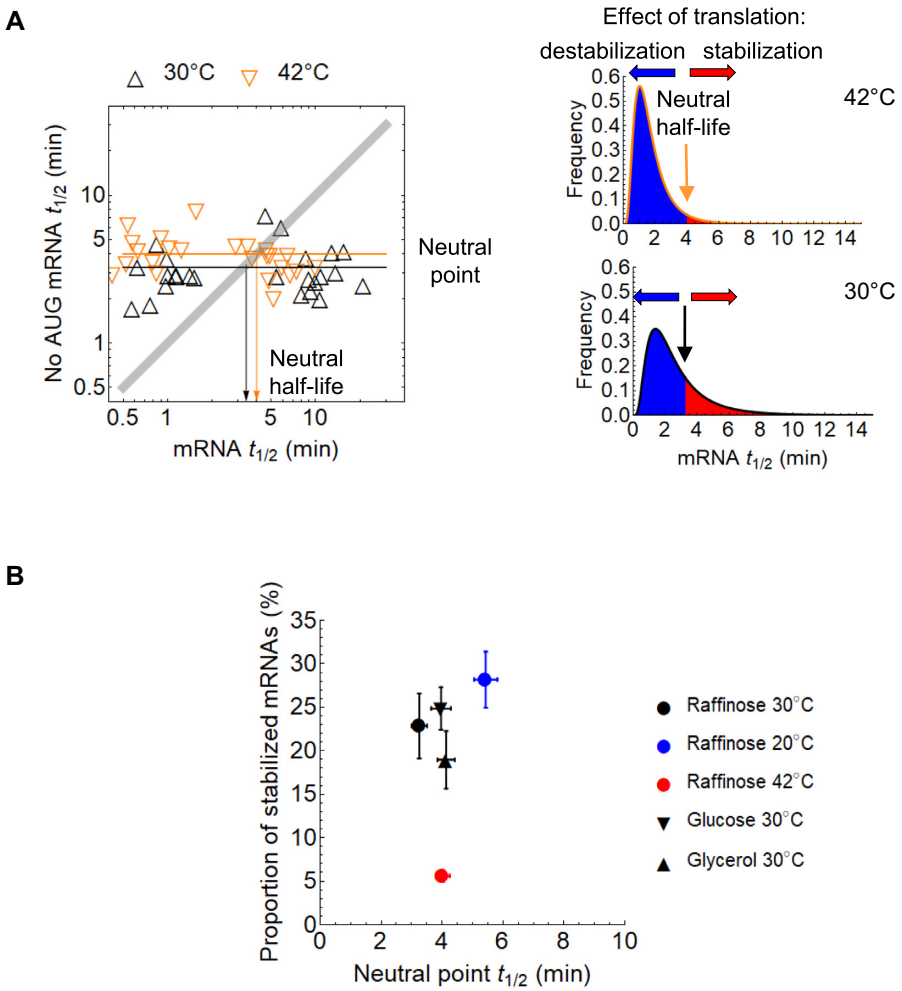

Figure 3. Global effect of temperature on the turnover of translated mRNAs. (**A**) The half-life of the mRNA with and without AUG codons in cells grown in raffinose at 30˚C or 42˚C. The neutral point denotes the mean no-AUG half-life (horizontal line in the left panel). The right panels indicate the probability density functions fitted to the half-lives of the representative mRNA set. (**B**) The percentage of stabilized mRNAs and the location of the neutral point in different growth conditions (5.5, 3.3 and 4.0 min for raffinose at 20˚, 30˚C and 42˚C; 3.9 and 4.2 min for glucose and glycerol, respectively). The error bars represent the standard error obtained by bootstrapping.

association is found also for Ser (47) (Supplementary Data S3). Asn and Ser also act as acceptor sites for glycosylation: Asn for N-glycosylation and Ser for O-glycosylation, and strongly glycosylated proteins reach the cell membrane and cell wall via the secretory pathway. The cell wall integrity signaling has been long known to be involved in the adaptation to growth at elevated temperature (48).

We summed up the dtCSCs for each mRNA and ranked them according the ∑dtCSC. mRNAs with the most negative ∑dtCSC often encoded cell membrane and cell wall proteins (Supplementary Figure S6C, D). Among the mRNAs with the most positive ∑dtCSC, there was a large number of mitochondrial proteins encoded by nuclear genes. We analyzed them in more detail (Figure 6A, B).

The mRNAs encoding Ser/Asn-rich membrane or membrane-associated proteins (*OST4*, *ECM33, MTL1* and *PST1,* Figure 6B) displayed temperature compensation.

To confirm the role of the relevant codons in the context of a typically long mRNA, we created mRNA mutant sequences of the *MTL1* gene. The *MTL1* coding sequence is 1656 bp long. The Mtl1 is serine-rich, heavily glycosylated membrane protein and act as stress sensor in the cell integrity pathway (49). To design the mutant sequence, we analyzed the significance of the differences between dtCSCs (Supplementary Text S2, Supplementary Tables S6 and S7), which is determined by the covariance of the frequency of the two codons to be compared and their dtCSC (50). The synonymous Tyr codons have positive dtCSC, whereas all but one Asn and Ser codons have negative dtCSC. Thus, the Asn and Ser codons generally promote temperature compensation, whereas Tyr codons promote temperature sensitization, but to an extent and significance that varies with the specific codon. Both Asn codons and four out of the six Ser codons differ significantly (at a significance level of $\alpha = 0.01$) from the Leu(CTT) and Tyr(TAT) codons (Supplementary Table S6). There are numerical but no significant differences between the synonymous codon of Asn, Ser or Tyr (Supplementary Table S7). This suggests that mRNA must be enriched in codons of specific amino acids to display temperature compensation or sensitization. We

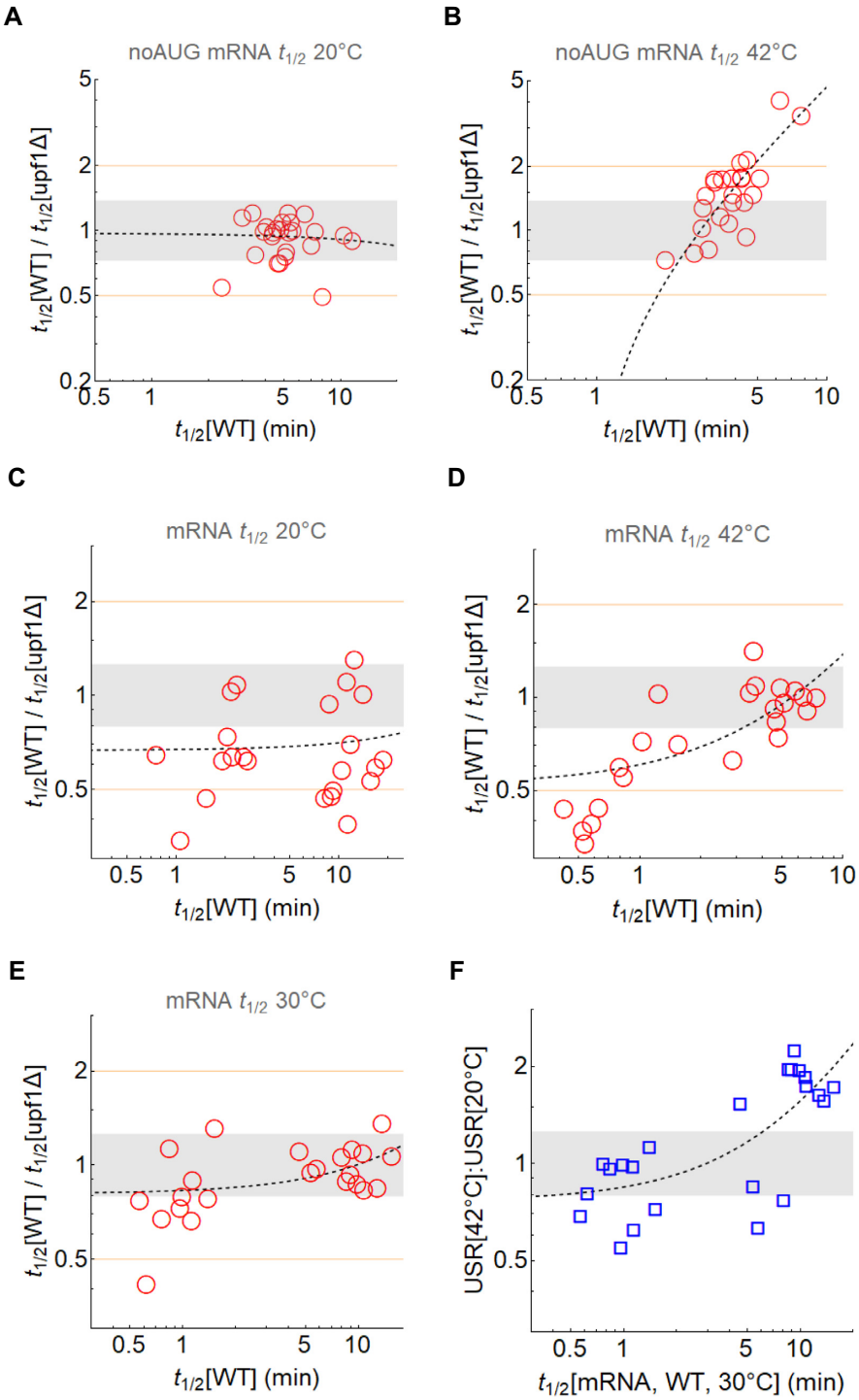

Figure 4. The half-lives of mRNAs and their no-AUG counterparts in *upf1Δ* cells. The half-life ($t_{1/2}$) of the set of stable and unstable mRNAs and their no-AUG counterparts was measured in WT and *upf1Δ* cells. The Upf1 stabilization ratio ($USR = t_{1/2}$[WT]/ $t_{1/2}$[*upf1Δ*]) reflects how the deletion of *UPF1* affects the half-life. A *USR* larger and less than one indicates stabilization and destabilization by *UPF1*, respectively. The gray band denotes a neutral ratio, $USR = 1$ and the thin solid lines denote twofold stabilization and destabilization by *UPF1*. The black dashed line is obtained with linear regression, which appears curved in the logarithmic plots. GM(*USR*) is the geometric mean of the USRs. The r_S and the associated *P*-value (*P*) are calculated for the two displayed variables. (**A**) no-AUG mRNAs at 20°C. GM(*USR*) = 0.92 ($N = 25$); $r_S = -0.09$, ($P = 0.67$). (**B**) no-AUG mRNAs at 42°C. GM(*USR*) = 1.48 ($N = 24$); $r_S = 0.82$ ($P = 4.6{\cdot}10^{-7}$). (**C**) mRNAs at 20°C. GM(*USR*) = 0.66 ($N = 23$); $r_S = 0.09$ ($P = 0.69$). (**D**) mRNAs at 42°C. GM(*USR*) = 0.74 ($N = 23$); $r_S = 0.73$ ($P = 7.9{\cdot}10^{-5}$). The interdecile ratio is reduced from 12 in WT cells to 4.9 in *upf1Δ* cells. (**E**) mRNAs at 30°C. GM(*USR*) = 0.90 ($N = 23$); $r_S = 0.50$ ($P = 0.014$). (**F**) The USR(42°C) : USR(20°C) ratio calculated for mRNAs. $r_S = 0.77$ ($P = 3.8{\cdot}10^{-5}$).

mutated the sequence so that the substituted codons have a significant difference in dtCSC. Specifically, the TAT (Tyr) codons were converted to AAC (Asn) in the SN-rich version. Since these mRNAs are already Asn/Ser rich, this change results in a small change relative to the WT gene. In order to create the Tyr-rich version, the opposite change was performed (Figure 6A). Furthermore, Ser (TCT) was changed to a Val(GTT) to avoid long segments of TAT (Tyr) codons; the GTT (Val) has a numerically positive dtCSC value with a significant difference in this mutation (Supplementary Table S7). The above changes affected nearly half of the *MTL1* sequence. Serine-rich proteins in the cell membrane and cell wall are targeted to their cellular location through the secretory pathway, and many of them have signal peptides, including the *MTL1*, which target them to the ER (49). Therefore, we created a second variant of the Tyr-rich sequence that lacked the signal peptide. The temperature compensation of the SN-rich *MTL1* mRNA was significant with respect to both Tyr-rich sequences, with and without the signal peptide sequence (Figure 6A).

The physiological response of the cell is determined by the abundance and activity of the proteins translated from the mRNAs. The stability coefficients of the codons (CSC) positively correlate with their translation efficiency at standard temperature (15). It can be hypothesized that there is a similar relation for dtCSC, as well. On the other hand, a strong translation at high temperature can be unfavorable because aggregation and degradation of proteins become prominent (51). Since the nascent proteins are in unfolded state, their high concentration at the ribosomes associated with a strongly translated mRNA can lead to aggregation at high temperatures (52,53). In the light of these conflicting expectations, we measured mRNA and protein levels upon heat shock to assess translation efficiency. For most proteins in this group, peptides were identified for the mass-spectrometric measurement using selective reaction monitoring (Materials and Methods) and their level was assessed 3 h after the shift to 42˚C. Among the examined proteins, the abundance of Pst1 and Mtl1 proteins increased while the level of the other proteins decreased or remained unchanged (Figure 6C). Interestingly, the mRNA expressed from the *PST1* and *MTL1* genes declined in the period from 30 to 90 min after the heat shock, but starting from a high level, indicating a pulse of transcription after the temperature shift. For all other genes, including *ECM33,* the mRNA levels rebounded after the initial decline in transcription. A comparison of the changes in protein and mRNA levels (Figure 6C) suggests that translation of most proteins is unchanged or decreased, which is consistent with the observed decline in translation of most proteins upon heat-shock (54,55).

To analyze the activity of a process in which proteins encoded with extreme $\sum$dtCSC play a major role in glycosylation and cell integrity, we measured the resistance of cells to a mixture of glucanases (zymolyase). An accelerated degradation of the cell wall by glucanases indicates a deficient cell wall resistance in cells in which a particular gene is deleted (Figure 6D). At 30˚C, none of the gene deletions resulted in deficient cell wall resistance when compared to cells containing control deletions (Δ*gal2* or Δ*gal3*). The cell wall sensitivity of the control cells changed from a ZRI of 10 at 30˚C to 10^{-1} at 42˚C. Thus, the control cells became significantly more resistant against the glucanases when the growth temperature was shifted from 30 to 42˚C, indicating an enhanced cell surface glycosylation in response to heat stress. The Δ*ost4* and Δ*ecm33* cells had deficient cell wall resistance at 42˚C, showing that genes with temperature-compensating codons can promote cellular integrity. Ost4 (oligosaccharyltransferase 4) is a 36-amino acid residue microprotein involved in the N-glycosylation in the endoplasmic reticulum (56,57), while Ecm33 is a GPI-anchored protein anchored at the cell surface and may regulate glycosylation, as well (58). Its homologue in *Candida albicans* is involved in cell-host interaction (59). Even though we expected the mitochondrial genes to act simply as control genes, their deletion resulted in an increased cell wall resistance. For Δ*pet100* (chaperone of cytochrome *c* oxidase) and Δ*cox14* (cytochrome *c* oxidase), this effect was evident at 30˚C while for Δ*qcr6* (cytochrome *c* reductase 6) at 42˚C. The deletion of other genes did not have significant effect. These results (Figure 6C, D) suggest that the increase in the activity or the physiological response associated with the relevant proteins, such as Ecm33, rather than their abundance promotes cell integrity upon heat shock.

DISCUSSION

The measurement of half-lives under stressful conditions, such as heat shock, is challenging due to the interaction of stress and the perturbations introduced by the specific methods of measuring half-lives. In the first part of our work, we showed that mRNA turnover can be measured reliably with the multiplexed gene control (MGC) method even under stressful conditions, as evidenced by the highly correlated half-lives measured over a wide temperature range (Figure 1B). This gradual change with temperature is in contradiction to the massive, abrupt changes reported by other studies which otherwise use methods that are consistent with one another at standard temperature (Figure 1D). There may be several reasons why the short-pulse metabolic labelling (cDTA) detects dramatic changes in mRNA stability upon a mild heat shock (37˚C). Cell density twice as high was used in the cDTA study, and the cells may be more prone to enter the stationary state. Furthermore, the 4-thiouracil used for the metabolic labelling of RNA in the cDTA induces the formation of P-bodies (30), as does heat stress. Thus, together, they can enhance the sequestration of mRNAs in the P-bodies, which would explain the slower decay rate in the 37˚C cDTA dataset. Perturbations induced by other methods, such as the transcriptional inhibition and the cell wall digestion in the runoff experiments, imitate heat shock (17), which may explain why the genetic run-on (GRO) and the cDTA datasets do not correlate even under standard conditions. At very high temperatures (46–47˚C), the proteins start to denature and aggregate, which is likely to lead to slower degradation (51,60).

Our MGC measurements revealed that mRNA turnover is fast in all examined conditions, and short median half-life (2.9 min) was observed even in glycerol, in which cell growth is slow, indicating that the rates of mRNA turnover and cell growth can be decoupled. The strong correlations indicate that the overall RNA degradation program is robust to changes in growth conditions.

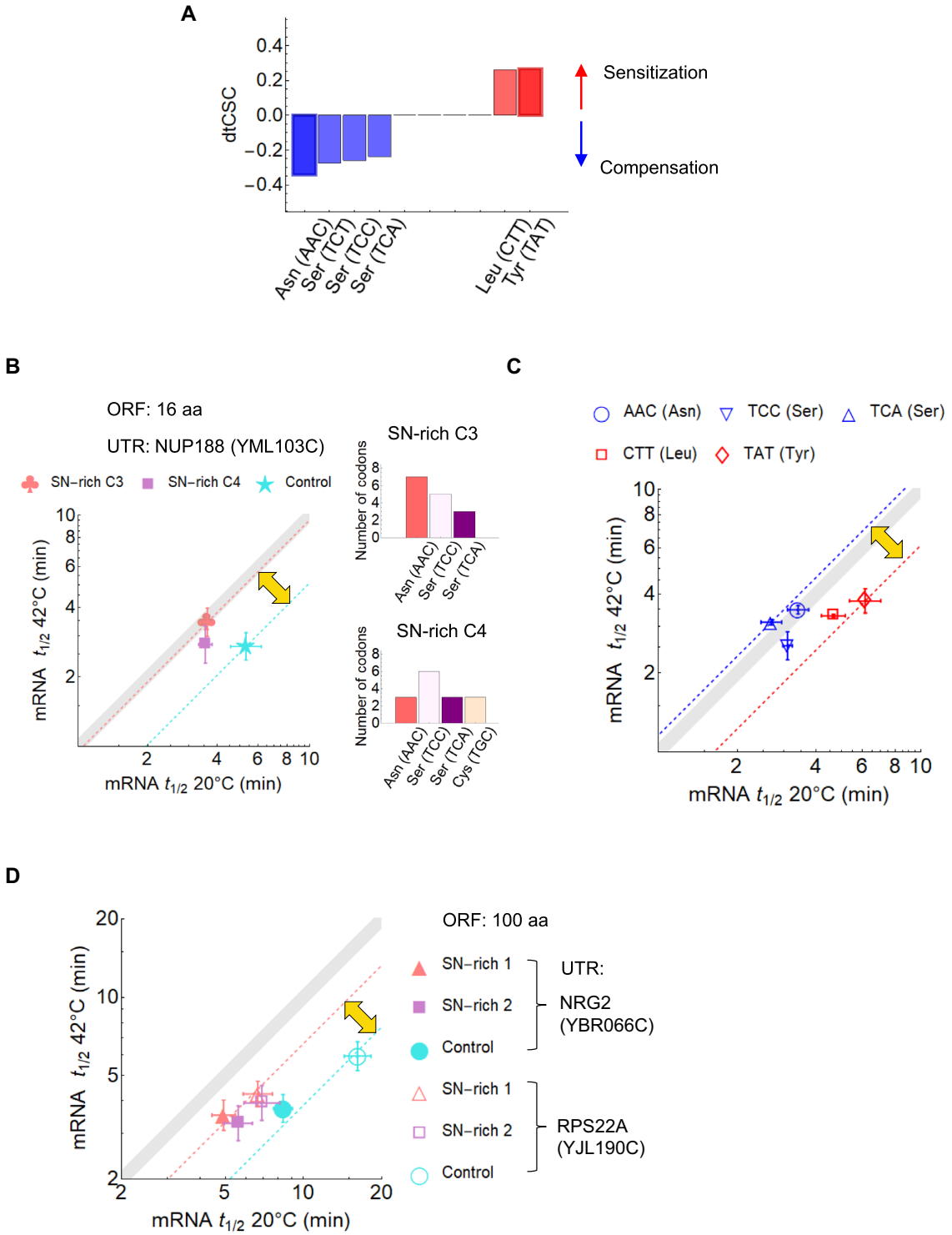

Figure 5. Codon-dependence of temperature adaptation in RNA degradation. (**A**) The dtCSC values calculated based on the representative and stable-unstable mRNA sets ($N = 95$). *P*-values are given for the corresponding Spearman rank correlation due to the deviation from normality: Asn(AAC) 0.0003; Tyr(TAT) 0.006; Leu(CTT) 0.010; Ser(TCC) 0.014, Ser(TCT) 0.016 and Ser(TCA) 0.038. Associations having *P*-values <0.01 are indicated by thick edges. (**B**) The half-lives of the mRNAs expressed from synthetic genes comprise 15 amino acids between the start and stop codons. The bar plots show the composition of the two Ser/Asn-rich genes, consisting of three (C3) and four (C4) different codons. The control gene (star) contains three copies of each of the following codons, with the dtCSC given in parenthesis: GAA (Glu, 0.03), GCA (Ala, 0.19); GGA, GGC and GGT (Gly; 0.15, 0.1 and 0.07). The error bars indicate standard errors ($n = 3$ independent experiments). The regression lines (dashed lines flanking the double-headed arrow) are calculated for the constructs with the largest difference in the half-lives. The temperature compensation of the SN-rich C3 mRNAs relative to the control (the ratio of the slopes of the dashed lines) is 1.87. (**C**) The half-lives of the mRNAs expressed from synthetic genes encode 14 identical amino acids and a methionine (start codon). The error bars indicate standard errors ($n = 3$ independent experiments). (**D**) The half-lives of mRNAs expressed from synthetic genes encoding 100 amino acids long proteins were inserted between the *NRG2* or *RPS22A* UTRs. The error bars indicate standard errors ($n = 3$).

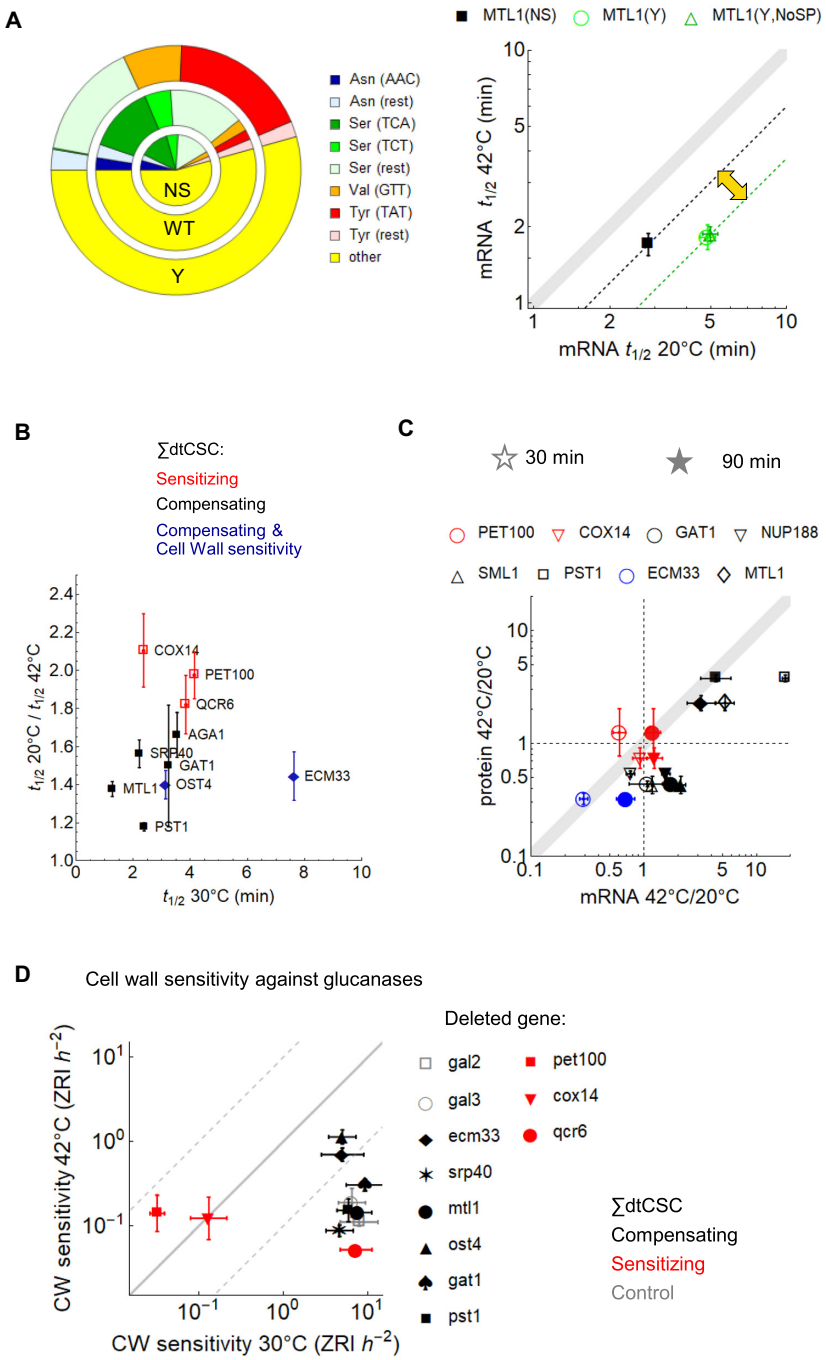

Figure 6. Functional relevance of enrichment of mRNAs in Asn and Ser codons. (**A**) The role of Asn, Ser and Tyr codons in the temperature compensation of the *MTL1* mRNA degradation. The codon composition of the Asn/Ser-rich (NS), WT and Tyr-rich (Y) sequences are shown in the pie charts. The NoSP denotes the construct with no signal peptide sequence. The error bars denote standard errors calculated from three biological replicates. The *P*-values were calculated for the log ratios of the half-life measured at 20 to that at 42˚C for the *t*-test: $P = 0.028$ for *MTL1*(NS) versus (Y) and $P = 0.013$ for *MTL1*(NS) vs (Y, No SP). Using Mann–Whitney yields $P = 0.029$ for both pairs. (**B**) The ratio of half-lives measured at 20 and 42˚C (standard error, $n = 3$) for the mRNAs enriched in temperature-compensating or temperature-sensitizing codons. The mRNAs are marked with multiple stop codons. The temperature-compensating mRNAs encoding genes responsible for the resistance against zymolyase are shown in dark blue. (**C**) Fold change of protein and mRNA levels measured at 20 versus 42˚C ($n = 3$ replicates). Proteins were measured 3 h after shifting the temperature to 42˚C, whereas the corresponding mRNAs were measured at 30 (empty symbols) and 90 (full symbols) min after the shift. Each gene is denoted by an empty and full symbol, which refer to the same protein measurement. This timing allows the typically slowly degrading proteins to integrate rapid changes in the amount of mRNA over the previous period. The thick gray line denotes equal change of protein and mRNA levels, which indicates that translation remains constant provided the protein half-life and transcription do not change. (**D**) The cell wall (CW) sensitivity against glycosidases (zymolyase rate index, ZRI) for cells in which the indicated genes are deleted. The full gray line indicates the same sensitivity at 30 and 42˚C. The upper and lower gray dashed lines denote 10 times higher and lower sensitivity at 42˚C, respectively. The *Δgal2* and *Δgal3* cells were used as control deletions (gray). The error bars denote the standard error from $n = 3$ biological replicates for cells grown at 30˚C, and $n = 5$ at 42˚C. Significant differences (Mann–Whitney) relative to the control cells (*Δgal2*, *Δgal3*) were found for *Δecm33* ($P = 0.006$, 0.012), *Δost4* ($P = 0.006$) and *Δqcr6* ($P = 0.012$) cells at 42˚C. For *Δgat1* $P = 0.006$ (vs *Δgal2*) and 0.094 (vs *Δgal3*).

Capitalizing on the reliability of the MGC, we examined in the second part of our work how translation affects the mRNA degradation at different temperatures by mutating all the start codons of the mRNA. In this way, we obviated the perturbations introduced by translation inhibitors or mutations that affect cell physiology. Much of the debate so far has centered on the question as to whether translation stabilizes or destabilizes mRNAs (31). mRNAs with optimal codons have long half-lives, while mRNAs with non-optimal codons have short half-lives due to the lower translational efficiency. By linear extrapolation of this relationship, it is expected that a further decrease in translation by eliminating translational initiation will result in very short half-lives. Intriguingly, the half-life of no-AUG mRNAs exceeded that of the unstable mRNAs, but ranked below the stable mRNAs. Accordingly, future studies have to identify molecular mechanisms that are consistent with this more general, nonlinear model, which does not view translation exclusively as either an mRNA stabilizing or a destabilizing process.

By calculating the average half-life of the no-AUG mRNAs, we obtained the neutral point (Figure 3), which divides the mRNA population into two subpopulations. About 20–25% of mRNAs are stabilized by translation, which is in good agreement with the analyses showing that one third of mRNAs of the genome are enriched in optimal codons (15). The proportion of translationally stabilized mRNAs remains relatively constant at 30˚C despite the wide variations in the growth rate of cells cultured in different carbon sources (Figure 1). Heat shock was the only one under the conditions tested that changed substantially this proportion (Figure 3B): translation stabilizes a mere 5% of mRNAs at 42˚C. At the same time, this subpopulation differed more strongly from the rest of the population (Figure 3A), which is also evidenced by the small standard error of the estimated subpopulation size (Figure 3B).

In principle, the proportion of translationally stabilized mRNAs can be changed directly by (de)stabilizing mRNAs or indirectly by shifting the neutral half-life. Our results suggest that Upf1 contributes to both of these modes. Upf1 is one of the up-frameshift (UPF) factors that target mRNAs with premature stop codons to nonsense mediated decay. The prototypical example of the Upf targets are the pre-mRNAs leaked into the cytoplasm, which contain premature stop codons in the retained introns. However, the majority of genes that increase their expression in response to the deletion of the *UPF* genes do not contain premature stop codons (44). It has been suggested that some of these mRNAs undergo poor start codon scanning during translation initiation, and the NMD is activated due to the start of translation in a nonsense frame. Furthermore, many of these mRNAs are enriched in non-optimal codons (61), which usually also destabilize mRNAs. Recently, non-classical functions of Upf1 have been described in mammalian cells that do not even require translational termination (62). For example, Upf1 can recognize highly structured mRNAs, typically in the noncoding regions (UTR).

Under the standard conditions (30˚C), only one out of the 23 mRNAs that comprised the set of stable and unstable mRNAs underwent a more than twofold stabilization in *upf1Δ* cells (Figure 4D): the *YML107C* (*PML39*). Pml39 is required for the nuclear retention of unspliced pre-mRNAs (63). In a high-throughput study, the deletion of the *UPF* genes tripled the expression of *YML107C* (*PML39*) (44,61), and this was the only mRNA among the 23 mRNAs whose expression more than doubled. This agreement is surprisingly good since a direct comparison between half-lives and steady-state expression levels is limited by the buffering effect of feedback loops that are activated when genes involved in RNA degradation and processing are deleted (20). *PML39* is an intronless gene, and the targeting of the *PML39* mRNA by Upf1 to degradation may represent a feedback loop that prevents the NMD pathway from becoming saturated by retaining unspliced mRNAs in the nucleus.

Interestingly, the Upf1 has a stronger effect on mRNA turnover at both low (20˚C) and high (42˚C) temperatures than at 30˚C (Figure 4C–E). The involvement of Upf1 in temperature adaptation is mediated by two different mechanisms. Due to a non-classical function, Upf1 stabilizes untranslated mRNAs upon heat-shock, which reduces the proportion translationally stabilized mRNAs indirectly. Many mRNAs in this subpopulation are more likely to be destabilized at lower temperatures by Upf1. In this way, Upf1 provides a mechanism for temperature compensation by acting directly on mRNAs (Figures 4F and 7A). By the combination of these indirect and direct effects, the translationally stabilized mRNA subpopulation becomes more distinct from the rest of the population (Figure 3B). Thus, Upf1 is an extrinsic determinant of temperature adaptation of mRNA turnover.

In the third part of our work, we investigated how temperature affects mRNA stability through an intrinsic factor, the codon composition of the mRNA. While a large number of codons are stabilizing or destabilizing (16), only few codons contribute to temperature compensation or sensitization (Figure 5A). mRNA degradation can be fully or partially temperature compensated when the mRNA is enriched in specific codons (Asn and Ser). Conversely, a Tyr codon sensitizes mRNA degradation in response to temperature (Figure 7B).

mRNAs encoding Ser-rich cell surface proteins that are subject to temperature compensation display various expression patterns. The *MTL1* expression increases in a pulse-like manner upon heat shock, while *ECM33* expression declines. Heat shock evokes a succession of phases before cells enter the quiescent state. The abundance of mRNA and proteins varies over this period (Figure 6C) (51), which makes it difficult to quantify translation efficiency. Our data suggest that translation remains unchanged or declines for most of the mRNAs examined (Figure 6C). A reduction in translation upon heat shock has been observed in several studies (54,64). A counterintuitive benefit of diminished translation is demonstrated by the observations that translation inhibitors can improve the survival of cells exposed to high temperatures (52), presumably due to the alleviation of proteotoxicity (53). Accordingly, the activity of a protein or associated physiological response can gain in importance despite reduced translation, as evidenced by our observation that the resistance to glucanases is enhanced after a heat shock (Figure 6D). Whereas the *ECM33* does not contribute to cell wall resistance at 30˚C,

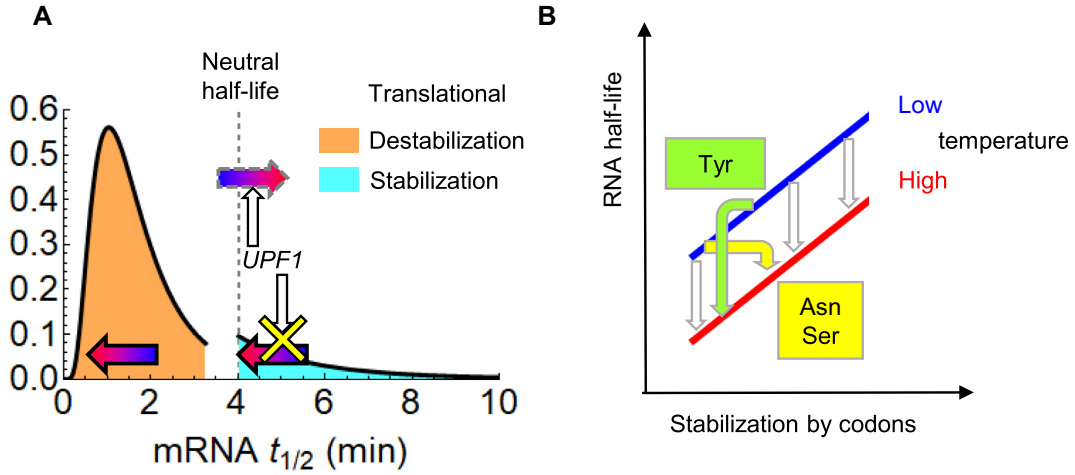

Figure 7. Scheme of the extrinsic and intrinsic determinants of the temperature adaptation of mRNA degradation. (**A**) Extrinsic determinants. Translation stabilizes mRNAs with a half-life greater than the neural half-life but below that destabilizes them. The gradient arrows indicate processes associated with a shift from low to high temperature. Heat shock reduces the proportion of translationally stabilized mRNAs indirectly because Upf1 increases the neutral half-life. At the same time, the increase in temperature buffers the destabilizing activity of Upf1 against some of the translationally stabilized mRNAs (cross). Consequently, the degradation of mRNAs is partially temperature compensated. (**B**) Codons are the intrinsic determinants of mRNAs temperature adaptation. Most codons do not change their stabilizing effect significantly upon temperature shift (gray arrows). However, specific Asn and Ser codons buffer the increase in the mRNA degradation rate as the temperature rises (compensation, bent horizontal arrow). On the other hand, a Tyr codon amplifies the temperature-induced change in mRNA stability (sensitization, bent vertical arrow).

it does so at 42˚C despite the reduced *ECM33* transcription and/or translation.

We will discuss two hypothetical mechanisms, the activity of the decoding tRNAs and the targeting of mRNAs to specific cell organelles or aggregates, which can explain temperature compensation of mRNAs enriched in these codons.

The stability coefficients of the mRNA codons correlate well with the abundance and translational adaption index tAi of the tRNA that decode them ($r = 0.6$ to 0.7). Temperature shift alters the abundance, covalent modifications or confirmation of tRNAs (65,66), which may underlie the codon-dependence of thermal adaptation. In principle, these mechanisms can destabilize mRNAs more at lower temperatures than at high temperatures, providing an alternative temperature compensation mechanism. The sequence context of the codons can also influence mRNA decay. The translation of repetitive sequences, often encoding identical amino acids, has been shown to alter the elongation rate (67,68), which can indirectly influence mRNA stability (16). This may lead to nonlinear relationships between the translation efficiency of individual codons and mRNA stability. Analogously, the degradation of mRNAs enriched in temperature-compensating or -sensitizing codons may be influenced by the local density of the codons and the nature of encoded amino acids.

Localization can play a similarly important role. Ser-rich proteins are targeted via the endoplasmic reticulum (ER) and the secretory pathway to the cell membrane and cell wall (47), which is preceded by the association of the corresponding mRNA with the ER. The induction of secretory pathway components in yeast can increase mRNA stability (69). Glycosylation of the proteins in the ER facilitates protein folding in general, and promotes cellular integrity at higher temperatures (70,71).

In addition to targeting to organelles, aggregation can also promote localization. P-bodies and stress granules are enriched in Asn-containing low complexity domains (47). Asn-richness promotes assembly of self-templating amyloids (72), which may contribute to the formation of ribonucleoprotein aggregates. The ratio of Ser to Tyr plays is an important determinant of aggresome formation *in vitro* (73). Interestingly, the C-terminal domain of the Lsm4 protein, which is responsible for the formation of P-bodies and aggregates into amyloids (72), is highly enriched in asparagine (*N*, 36%) and moderately enriched in serine (S, 17%), and the gene lacks the Tyr(TAT) codon (74). This composition is similar to the synthetic sequences encoding Asn/Ser-rich proteins analyzed in our study. The C-terminal domain of Lsm4p is the P-body component that is most highly enriched in asparagine (Supplementary Data S3).

While P-bodies and stress granules share important similarities, there are stress-specific differences in composition and assembly (75,76). Typically, they are viewed as storage sites of translationally repressed mRNAs. However, translation has been observed in these granules, suggesting that repression is partial and not complete (77). Temperature compensation would then simply result from the storage and stabilization of these mRNAs in ribonucleoprotein aggregates, in which translation is reduced. Since more and more proteins aggregate with increasing temperature (51), it remains to be clarified whether and which form of ribonucleoprotein aggregates are relevant for temperature compensation. Interestingly, Upf1p can target both nonsense and normal mRNAs to P-bodies, without promoting the degradation of normal mRNA (78). Similarly, Upf1 promotes the formation of aggresomes, which accumulate misfolded proteins during heat stress (51,79). Such a non-classical function of Upf1 can explain the stabilization of untranslated no-AUGs upon heat shock. The physiological relevance of

the involvement of Upf1 in temperature adaptation is underlined by a study showing that Upf1 mutant cells have increased heat sensitivity (80). Thus, both the extrinsic and intrinsic determinants of temperature adaptation overlap with P-body components. Whereas the extrinsic determinant, Upf1 may target mRNAs to P-bodies directly, the formation of aggregates containing mRNAs enriched in compensating codons may be co-translational since Asn-rich proteins are prone to aggregate, a process that can particularly affect nascent proteins at high temperature. Interestingly, the two Asn/Ser-rich cellular compartments interact, since the cell wall integrity pathway controls P-body assembly upon cell wall stress (10).

Our results with consistent half-lives over a broad range of temperatures provide insight into the temperature adaptation under physiological conditions and into the early phase of heat shock response when cells still divide. This facilitated the identification of the regulators and the sequence specific determinants of the temperature adaptation of mRNA degradation.

DATA AVAILABILITY

Data are available as supplementary data.

SUPPLEMENTARY DATA

Supplementary Data are available at NAR Online.

ACKNOWLEDGEMENTS

We thank David Sommer, Melissa Langlois, Patrick Romann, Vinciane Fluhler, Phillippe Demougin, Mara Julseth, Sayanur Rahman and Chandraday Prodhan for the experimental help, Alexander Schmidt (Proteomics Core Facility) for the proteomics measurements, Stephen N. Floor for helpful discussion, and Ertugrul Ozbudak for comments on the manuscript.

Author contributions: A. B. designed the experiments and wrote the manuscript. V.J., D.T. and A.B. analyzed the data. S.W., S.V., V.J. and E.C.V performed the experiments.

FUNDING

StoNets RTD from SystemsX.ch. (in part). Funding for open access charge: University of Basel.

Conflict of interest statement. None declared.

REFERENCES

1. Alster,C.J., Fischer,J.C., Allison,S.D. and Treseder,K.K. (2020) Embracing a new paradigm for temperature sensitivity of soil microbes. *Glob. Chang. Biol.*, **26**, 3221–3229.
2. Kortmann,J. and Narberhaus,F. (2012) Bacterial RNA thermometers: molecular zippers and switches. *Nat. Rev. Microbiol.*, **10**, 255–265.
3. Tomita,J., Nakajima,M., Kondo,T. and Iwasaki,H. (2005) No transcription-translation feedback in circadian rhythm of KaiC phosphorylation. *Science*, **307**, 251–254.
4. Robertson,R.M. and Money,T.G. (2012) Temperature and neuronal circuit function: compensation, tuning and tolerance. *Curr. Opin. Neurobiol.*, **22**, 724–734.
5. Irvine,S.Q. (2020) Embryonic canalization and its limits-A view from temperature. *J. Exp. Zool. B Mol. Dev. Evol.*, **334**, 128–144.
6. Zinani,O.Q.H., Keseroglu,K., Ay,A. and Ozbudak,E.M. (2021) Pairing of segmentation clock genes drives robust pattern formation. *Nature*, **589**, 431–436.
7. Chen,Y.H. and Coller,J. (2016) A Universal Code for mRNA Stability? *Trends Genet.*, **32**, 687–688.
8. Bazzini,A.A., Del Viso,F., Moreno-Mateos,M.A., Johnstone,T.G., Vejnar,C.E., Qin,Y., Yao,J., Khokha,M.K. and Giraldez,A.J. (2016) Codon identity regulates mRNA stability and translation efficiency during the maternal-to-zygotic transition. *EMBO J.*, **35**, 2087–2103.
9. Mishima,Y. and Tomari,Y. (2016) Codon Usage and 3′ UTR Length Determine Maternal mRNA Stability in Zebrafish. *Mol. Cell*, **61**, 874–885.
10. Garcia,R., Pulido,V., Orellana-Munoz,S., Nombela,C., Vazquez de Aldana,C.R., Rodriguez-Pena,J.M. and Arroyo,J. (2019) Signalling through the yeast MAPK Cell Wall Integrity pathway controls P-body assembly upon cell wall stress. *Sci. Rep.*, **9**, 3186.
11. Luo,Y., Na,Z. and Slavoff,S.A. (2018) P-Bodies: composition, properties, and functions. *Biochemistry*, **57**, 2424–2431.
12. Balagopal,V. and Parker,R. (2009) Polysomes, P bodies and stress granules: states and fates of eukaryotic mRNAs. *Curr. Opin. Cell Biol.*, **21**, 403–408.
13. Herrick,D., Parker,R. and Jacobson,A. (1990) Identification and comparison of stable and unstable mRNAs in Saccharomyces cerevisiae. *Mol. Cell. Biol.*, **10**, 2269–2284.
14. Wada,T. and Becskei,A. (2017) Impact of Methods on the Measurement of mRNA Turnover. *Int. J. Mol. Sci.*, **18**, 2723.
15. Carneiro,R.L., Requiao,R.D., Rossetto,S., Domitrovic,T. and Palhano,F.L. (2019) Codon stabilization coefficient as a metric to gain insights into mRNA stability and codon bias and their relationships with translation. *Nucleic Acids Res.*, **47**, 2216–2228.
16. Presnyak,V., Alhusaini,N., Chen,Y.H., Martin,S., Morris,N., Kline,N., Olson,S., Weinberg,D., Baker,K.E., Graveley,B.R. *et al.* (2015) Codon optimality is a major determinant of mRNA stability. *Cell*, **160**, 1111–1124.
17. Adams,C.C. and Gross,D.S. (1991) The yeast heat shock response is induced by conversion of cells to spheroplasts and by potent transcriptional inhibitors. *J. Bacteriol.*, **173**, 7429–7435.
18. Malik,I., Qiu,C., Snavely,T. and Kaplan,C.D. (2017) Wide-ranging and unexpected consequences of altered Pol II catalytic activity in vivo. *Nucleic Acids Res.*, **45**, 4431–4451.
19. Baudrimont,A., Voegeli,S., Viloria,E.C., Stritt,F., Lenon,M., Wada,T., Jaquet,V. and Becskei,A. (2017) Multiplexed gene control reveals rapid mRNA turnover. *Sci. Adv.*, **3**, e1700006.
20. Sun,M., Schwalb,B., Schulz,D., Pirkl,N., Etzold,S., Lariviere,L., Maier,K.C., Seizl,M., Tresch,A. and Cramer,P. (2012) Comparative dynamic transcriptome analysis (cDTA) reveals mutual feedback between mRNA synthesis and degradation. *Genome Res.*, **22**, 1350–1359.
21. Reimann,C., Filzmoser,P. and Garrett,R.G. (2005) Background and threshold: critical comparison of methods of determination. *Sci. Total Environ.*, **346**, 1–16.
22. Blewett,N., Coller,J. and Goldstrohm,A. (2011) A quantitative assay for measuring mRNA decapping by splinted ligation reverse transcription polymerase chain reaction: qSL-RT-PCR. *RNA*, **17**, 535–543.
23. Pelechano,V., Wei,W. and Steinmetz,L.M. (2013) Extensive transcriptional heterogeneity revealed by isoform profiling. *Nature*, **497**, 127–131.
24. Raj,A. and Tyagi,S. (2010) Detection of individual endogenous RNA transcripts in situ using multiple singly labeled probes. *Methods Enzymol.*, **472**, 365–386.
25. Baudrimont,A., Jaquet,V., Wallerich,S., Voegeli,S. and Becskei,A. (2019) Contribution of RNA Degradation to Intrinsic and Extrinsic Noise in Gene Expression. *Cell Rep.*, **26**, 3752–3761.
26. Gencoglu,M., Schmidt,A. and Becskei,A. (2017) Measurement of in vivo protein binding affinities in a signaling network with mass spectrometry. *ACS Synth. Biol.*, **6**, 1305–1314.
27. Stringer,C., Wang,T., Michaelos,M. and Pachitariu,M. (2020) Cellpose: a generalist algorithm for cellular segmentation. *Nat. Methods*, **18**, 100–106.
28. Ovalle,R., Lim,S.T., Holder,B., Jue,C.K., Moore,C.W. and Lipke,P.N. (1998) A spheroplast rate assay for determination of cell wall integrity in yeast. *Yeast*, **14**, 1159–1166.

29. Cherry,J.M., Hong,E.L., Amundsen,C., Balakrishnan,R., Binkley,G., Chan,E.T., Christie,K.R., Costanzo,M.C., Dwight,S.S., Engel,S.R. *et al.* (2012) Saccharomyces Genome Database: the genomics resource of budding yeast. *Nucleic Acids Res.*, **40**, D700–D705.
30. Eshleman,N., Luo,X., Capaldi,A. and Buchan,J.R. (2020) Alterations of signaling pathways in response to chemical perturbations used to measure mRNA decay rates in yeast. *RNA*, **26**, 10–18.
31. Huch,S. and Nissan,T. (2014) Interrelations between translation and general mRNA degradation in yeast. *Wiley Interdiscip. Rev. RNA*, **5**, 747–763.
32. Fleischmann,J., Rocha,M.A., Hauser,P.V., Gowda,B.S. and Pilapil,M.G.D. (2020) Exonuclease resistant 18S and 25S ribosomal RNA components in yeast are possibly newly transcribed by RNA polymerase II. *BMC Mol. Cell Biol.*, **21**, 59.
33. Gibney,P.A., Lu,C., Caudy,A.A., Hess,D.C. and Botstein,D. (2013) Yeast metabolic and signaling genes are required for heat-shock survival and have little overlap with the heat-induced genes. *Proc. Natl. Acad. Sci. U.S.A.*, **110**, E4393–E4402.
34. Zakrzewska,A., van Eikenhorst,G., Burggraaff,J.E., Vis,D.J., Hoefsloot,H., Delneri,D., Oliver,S.G., Brul,S. and Smits,G.J. (2011) Genome-wide analysis of yeast stress survival and tolerance acquisition to analyze the central trade-off between growth rate and cellular robustness. *Mol. Biol. Cell*, **22**, 4435–4446.
35. Garcia-Martinez,J., Delgado-Ramos,L., Ayala,G., Pelechano,V., Medina,D.A., Carrasco,F., Gonzalez,R., Andres-Leon,E., Steinmetz,L., Warringer,J. *et al.* (2016) The cellular growth rate controls overall mRNA turnover, and modulates either transcription or degradation rates of particular gene regulons. *Nucleic Acids Res.*, **44**, 3643–3658.
36. Izawa,S., Kita,T., Ikeda,K. and Inoue,Y. (2008) Heat shock and ethanol stress provoke distinctly different responses in 3′-processing and nuclear export of HSP mRNA in Saccharomyces cerevisiae. *Biochem. J.*, **414**, 111–119.
37. Castells-Roca,L., Garcia-Martinez,J., Moreno,J., Herrero,E., Belli,G. and Perez-Ortin,J.E. (2011) Heat shock response in yeast involves changes in both transcription rates and mRNA stabilities. *PLoS One*, **6**, e17272.
38. Luo,Y., Schofield,J.A., Simon,M.D. and Slavoff,S.A. (2020) Global Profiling of Cellular Substrates of Human Dcp2. *Biochemistry*, **59**, 4176–4188.
39. Yu,X. and Warner,J.R. (2001) Expression of a micro-protein. *J. Biol. Chem.*, **276**, 33821–33825.
40. Kearse,M.G. and Wilusz,J.E. (2017) Non-AUG translation: a new start for protein synthesis in eukaryotes. *Genes Dev.*, **31**, 1717–1731.
41. Chang,K.J. and Wang,C.C. (2004) Translation initiation from a naturally occurring non-AUG codon in Saccharomyces cerevisiae. *J. Biol. Chem.*, **279**, 13778–13785.
42. Chen,S.J., Lin,G., Chang,K.J., Yeh,L.S. and Wang,C.C. (2008) Translational efficiency of a non-AUG initiation codon is significantly affected by its sequence context in yeast. *J. Biol. Chem.*, **283**, 3173–3180.
43. Eisenberg,A.R., Higdon,A.L., Hollerer,I., Fields,A.P., Jungreis,I., Diamond,P.D., Kellis,M., Jovanovic,M. and Brar,G.A. (2020) Translation Initiation Site Profiling Reveals Widespread Synthesis of Non-AUG-Initiated Protein Isoforms in Yeast. *Cell Syst.*, **11**, 145–160.
44. He,F., Li,X., Spatrick,P., Casillo,R., Dong,S. and Jacobson,A. (2003) Genome-wide analysis of mRNAs regulated by the nonsense-mediated and 5′ to 3′ mRNA decay pathways in yeast. *Mol. Cell*, **12**, 1439–1452.
45. Bonde,M.M., Voegeli,S., Baudrimont,A., Seraphin,B. and Becskei,A. (2014) Quantification of pre-mRNA escape rate and synergy in splicing. *Nucleic Acids Res.*, **42**, 12847–12860.
46. Brar,G.A., Yassour,M., Friedman,N., Regev,A., Ingolia,N.T. and Weissman,J.S. (2012) High-resolution view of the yeast meiotic program revealed by ribosome profiling. *Science*, **335**, 552–557.
47. Cascarina,S.M. and Ross,E.D. (2018) Proteome-scale relationships between local amino acid composition and protein fates and functions. *PLoS Comput. Biol.*, **14**, e1006256.
48. Levin,D.E. (2011) Regulation of cell wall biogenesis in Saccharomyces cerevisiae: the cell wall integrity signaling pathway. *Genetics*, **189**, 1145–1175.
49. Petkova,M.I., Pujol-Carrion,N. and de la Torre-Ruiz,M.A. (2012) Mtl1 O-mannosylation mediated by both Pmt1 and Pmt2 is important for cell survival under oxidative conditions and TOR blockade. *Fungal Genet. Biol.*, **49**, 903–914.
50. Steiger,J.H. (1980) Tests for Comparing Elements of a Correlation Matrix. *Psychol. Bull.*, **87**, 245–251.
51. Muhlhofer,M., Berchtold,E., Stratil,C.G., Csaba,G., Kunold,E., Bach,N.C., Sieber,S.A., Haslbeck,M., Zimmer,R. and Buchner,J. (2019) The Heat Shock Response in Yeast Maintains Protein Homeostasis by Chaperoning and Replenishing Proteins. *Cell Rep.*, **29**, 4593–4607.
52. Jarolim,S., Ayer,A., Pillay,B., Gee,A.C., Phrakaysone,A., Perrone,G.G., Breitenbach,M. and Dawes,I.W. (2013) Saccharomyces cerevisiae genes involved in survival of heat shock. *G3 (Bethesda)*, **3**, 2321–2333.
53. Tye,B.W. and Churchman,L.S. (2021) Hsf1 activation by proteotoxic stress requires concurrent protein synthesis. *Mol. Biol. Cell*, **32**, 1800–1806.
54. Miller,M.J., Xuong,N.H. and Geiduschek,E.P. (1979) A response of protein synthesis to temperature shift in the yeast Saccharomyces cerevisiae. *Proc. Natl. Acad. Sci. U.S.A.*, **76**, 5222–5225.
55. Neef,D.W. and Thiele,D.J. (2009) Enhancer of decapping proteins 1 and 2 are important for translation during heat stress in Saccharomyces cerevisiae. *Mol. Microbiol.*, **73**, 1032–1042.
56. Shrimal,S. and Gilmore,R. (2019) Oligosaccharyltransferase structures provide novel insight into the mechanism of asparagine-linked glycosylation in prokaryotic and eukaryotic cells. *Glycobiology*, **29**, 288–297.
57. Chi,J.H., Roos,J. and Dean,N. (1996) The OST4 gene of Saccharomyces cerevisiae encodes an unusually small protein required for normal levels of oligosaccharyltransferase activity. *J. Biol. Chem.*, **271**, 3132–3140.
58. Pardo,M., Monteoliva,L., Vazquez,P., Martinez,R., Molero,G., Nombela,C. and Gil,C. (2004) PST1 and ECM33 encode two yeast cell surface GPI proteins important for cell wall integrity. *Microbiology*, **150**, 4157–4170.
59. Gil-Bona,A., Reales-Calderon,J.A., Parra-Giraldo,C.M., Martinez-Lopez,R., Monteoliva,L. and Gil,C. (2016) The Cell Wall Protein Ecm33 of Candida albicans is Involved in Chronological Life Span, Morphogenesis, Cell Wall Regeneration, Stress Tolerance, and Host-Cell Interaction. *Front. Microbiol.*, **7**, 64.
60. Hilgers,V., Teixeira,D. and Parker,R. (2006) Translation-independent inhibition of mRNA deadenylation during stress in Saccharomyces cerevisiae. *RNA*, **12**, 1835–1845.
61. Celik,A., Baker,R., He,F. and Jacobson,A. (2017) High-resolution profiling of NMD targets in yeast reveals translational fidelity as a basis for substrate selection. *RNA*, **23**, 735–748.
62. Lavysh,D. and Neu-Yilik,G. (2020) UPF1-Mediated RNA Decay-Danse Macabre in a Cloud. *Biomolecules*, **10**, 999.
63. Palancade,B., Zuccolo,M., Loeillet,S., Nicolas,A. and Doye,V. (2005) Pml39, a novel protein of the nuclear periphery required for nuclear retention of improper messenger ribonucleoparticles. *Mol. Biol. Cell*, **16**, 5258–5268.
64. Dever,T.E., Kinzy,T.G. and Pavitt,G.D. (2016) Mechanism and Regulation of Protein Synthesis in Saccharomyces cerevisiae. *Genetics*, **203**, 65–107.
65. Torrent,M., Chalancon,G., de Groot,N.S., Wuster,A. and Madan Babu,M. (2018) Cells alter their tRNA abundance to selectively regulate protein synthesis during stress conditions. *Sci. Signal*, **11**, eaat6409.
66. Lorenz,C., Lunse,C.E. and Morl,M. (2017) tRNA Modifications: Impact on Structure and Thermal Adaptation. *Biomolecules*, **7**, 35.
67. Tesina,P., Lessen,L.N., Buschauer,R., Cheng,J., Wu,C.C., Berninghausen,O., Buskirk,A.R., Becker,T., Beckmann,R. and Green,R. (2020) Molecular mechanism of translational stalling by inhibitory codon combinations and poly(A) tracts. *EMBO J.*, **39**, e103365.
68. Chandrasekaran,V., Juszkiewicz,S., Choi,J., Puglisi,J.D., Brown,A., Shao,S., Ramakrishnan,V. and Hegde,R.S. (2019) Mechanism of ribosome stalling during translation of a poly(A) tail. *Nat. Struct. Mol. Biol.*, **26**, 1132–1140.
69. Hyde,M., Block-Alper,L., Felix,J., Webster,P. and Meyer,D.I. (2002) Induction of secretory pathway components in yeast is associated with increased stability of their mRNA. *J. Cell Biol.*, **156**, 993–1001.

70. Lehrman,M.A. (2006) Stimulation of N-linked glycosylation and lipid-linked oligosaccharide synthesis by stress responses in metazoan cells. *Crit. Rev. Biochem. Mol. Biol.*, **41**, 51–75.
71. Cherepanova,N., Shrimal,S. and Gilmore,R. (2016) N-linked glycosylation and homeostasis of the endoplasmic reticulum. *Curr. Opin. Cell Biol.*, **41**, 57–65.
72. Halfmann,R., Alberti,S., Krishnan,R., Lyle,N., O'Donnell,C.W., King,O.D., Berger,B., Pappu,R.V. and Lindquist,S. (2011) Opposing effects of glutamine and asparagine govern prion formation by intrinsically disordered proteins. *Mol. Cell*, **43**, 72–84.
73. Kato,M., Han,T.W., Xie,S., Shi,K., Du,X., Wu,L.C., Mirzaei,H., Goldsmith,E.J., Longgood,J., Pei,J. *et al.* (2012) Cell-free formation of RNA granules: low complexity sequence domains form dynamic fibers within hydrogels. *Cell*, **149**, 753–767.
74. Reijns,M.A., Alexander,R.D., Spiller,M.P. and Beggs,J.D. (2008) A role for Q/N-rich aggregation-prone regions in P-body localization. *J. Cell Sci.*, **121**, 2463–2472.
75. Escalante,L.E. and Gasch,A.P. (2021) The role of stress-activated RNA-protein granules in surviving adversity. *RNA*, https://doi.org/10.1261/rna.078738.121.
76. Tishinov,K. and Spang,A. (2021) The mRNA decapping complex is buffered by nuclear localization. *J. Cell Sci.*, **134**, jcs259156.
77. Lui,J., Castelli,L.M., Pizzinga,M., Simpson,C.E., Hoyle,N.P., Bailey,K.L., Campbell,S.G. and Ashe,M.P. (2014) Granules harboring translationally active mRNAs provide a platform for P-body formation following stress. *Cell Rep.*, **9**, 944–954.
78. Sheth,U. and Parker,R. (2006) Targeting of aberrant mRNAs to cytoplasmic processing bodies. *Cell*, **125**, 1095–1109.
79. Park,Y., Park,J., Hwang,H.J., Kim,B., Jeong,K., Chang,J., Lee,J.B. and Kim,Y.K. (2020) Nonsense-mediated mRNA decay factor UPF1 promotes aggresome formation. *Nat. Commun.*, **11**, 3106.
80. Sinha,H., David,L., Pascon,R.C., Clauder-Munster,S., Krishnakumar,S., Nguyen,M., Shi,G., Dean,J., Davis,R.W., Oefner,P.J. *et al.* (2008) Sequential elimination of major-effect contributors identifies additional quantitative trait loci conditioning high-temperature growth in yeast. *Genetics*, **180**, 1661–1670.